

Pulsating subdwarf B stars observed with K2 during Campaign 7 and an examination of seismic group-properties.

M. D. Reed^{1,2*}, A. Slayton¹, A. S. Baran^{1,2,3}, J. H. Telting^{2,4,5}, R. H. Østensen^{1,2,6},

C. S. Jeffery⁷, M. Uzundag^{8,9}, S. Sanjayan^{2,10}

¹Department of Physics, Astronomy and Materials Science, Missouri State University, 901 S. National, Springfield, MO 65897, USA

²ARDASTELLA Research Group, Institute of Physics, Pedagogical University of Cracow, ul. Podchorążych 2, 30-084 Kraków, Poland

³Embry-Riddle Aeronautical University, Department of Physical Science, Daytona Beach, FL 32114, USA

⁴Nordic Optical Telescope, Rambla José Ana Fernández Pérez 7, 38711 Breña Baja, Spain

⁵Department of Physics and Astronomy, Aarhus University, Ny Munkegade 120, DK-8000 Aarhus C, Denmark

⁶Recogito AS, Storgaten 72, N-8200 Fauske, Norway

⁷Armagh Observatory and Planetarium, College Hill, Armagh BT61 9DG, N. Ireland

⁸Instituto de Física y Astronomía, Universidad de Valparaíso, Gran Bretaña 1111, Playa Ancha, Valparaíso 2360102, Chile

⁹European Southern Observatory, Alonso de Cordova 3107, Santiago, Chile

¹⁰Centrum Astronomiczne im. Mikołaja Kopernika, Polskiej Akademii Nauk, ul. Bartycka 18, 00-716 Warszawa, Polska

Accepted Received

ABSTRACT

We report the discovery of four new pulsating subdwarf B (sdBV) stars from Campaign 7 of the Kepler spacecraft’s K2 mission. EPICs 215776487, 217280630, 218366972, and 218717602 are all gravity (g)-mode pulsators and we also detect two pressure (p)-mode pulsations in EPIC 218717602. We detect asymptotic $\ell = 1$ sequences in all four stars, allowing us to identify nearly all of the g modes. We detect evenly-spaced frequency multiplets in EPIC 218717602 from which we determine a rotation period near seven days. Spectroscopic observations determine that EPIC 218366972 is in a 5.92 d binary with most likely a white dwarf companion of canonical mass while the others have no detected companions. As we detect no multiplets in EPIC 218366972, it is added to the growing list of subsynchronously rotating stars. With 40 Kepler-detected sdBV stars and a growing number of TESS publications, we update an examination of the group properties to provide direction for models. We notice a correlation between effective temperature and period of maximum pulsation amplitude, at least for g-mode pulsations, and update the previously-observed effective temperature – rotation period relation.

Key words:

Stars: oscillations – Stars: subdwarfs

1 INTRODUCTION

Kepler space telescope data have been fundamental in advances in asteroseismology. The original mission (K1) concluded with four years of nearly-uninterrupted single-instrument data. No comparable data set has ever previously been obtained. Kepler data do not suffer from daytime gaps nor differing instrumentation or observing sites trying to use multiple Earth longitudes to obtain complete coverage. There are no atmospheric effects and no Earth-orbiting complications (such as the South Atlantic Anomaly). The follow-on mission, K2, has similarly obtained heretofore unobtainable data sets, though of shorter (typically about 80 days) duration. The K2 mission observed 20 fields in the ecliptic plane, ingeniously using solar pressure to aid with pointing stability (Howell et al. 2014).

Those data have resulted in nearly 1,600 publications on

astrophysics unrelated to Kepler’s primary mission of discovering planets. An important area of contribution is asteroseismology. Asteroseismology uses pulsations to discern stellar structure and evolution. Prior to Kepler, horizontal branch asteroseismology, where we can explore compact, evolved cores undergoing helium fusion, was more effort than result. There were debates whether oscillations had been detected at all in red clump stars (solar-like oscillations). Amongst hot extreme horizontal branch stars, observations had done little to identify modes and hence constrain models.

Significant effort was expended trying to identify pulsation modes in pulsating sdB (sdBV) stars using follow-up longer-duration photometry (e.g. Reed et al. 2007), multicolour photometry (e.g. Randall et al. 2006), and time-resolved spectroscopy (e.g. Baran et al. 2010), with limited success. In large part, this was due to ground-based observations’ low-duty-cycle (typically < 30% coverage) or limited duration on larger facilities. Kepler and K2’s unique data sets allowed

* E-mail: MikeReed@missouristate.edu

observers to finally fully exploit these stars' pulsations with seismic analyses.

Subdwarf B stars pulsate in both pressure (p) and gravity (g) modes; with the hotter stars primarily p-mode dominated and the cooler stars predominantly g-mode-dominated pulsators. Typical p modes have periods of a few minutes with amplitudes rarely above 10 parts-per-thousand (ppt) while g modes have longer periods, typically 1-4 hours, with slightly lower amplitudes. The variable star classifications for sdBV stars are V361 Hya for p mode pulsators (Kilkenny et al. 1997), V1093 Her for g mode pulsators (Green et al. 2003), and DW Lyn (Schuh et al. 2006) for hybrid pulsators which pulsate in both p and g modes. These classifications have become less distinct as the majority of Kepler-observed sdBV stars have both types of pulsations. DW Lyn as a hybrid has two strong p-mode pulsations and only one g-mode pulsation yet for most of the Kepler-observed sdBV stars, the situation is reversed with more g modes observed than p modes. To distinguish which type of pulsation is dominant (in amplitude and number of detected pulsation periodicities), in this paper we use p+g and g+p for p and g-mode dominated hybrid pulsators, respectively. For a review of sdB and sdO stars, see Heber (2016), which includes some early Kepler results.

Seismic discoveries using K1 and K2 data obtained for sdBV stars include mode identifications using asymptotic g-mode-overtone period spacings (Reed et al. 2011) and rotationally-induced frequency multiplets (Baran et al. 2012). These two methods have provided around two thousand identified modes; to date, *every* Kepler-observed sdBV star which has been analyzed has had the majority of its periodicities associated with pulsation modes (where n represents radial overtones, ℓ the number of surface nodes, and m the azimuthal surface nodes). The most recent review of Kepler results for sdBV stars is Reed et al. (2018) and we examine group properties in §4.

In this paper we analyze four sdBV stars discovered during K2's Campaign 7 (C7) and place them in context with what has been detected so far. EPIC 215776487 (2MASS 19413850-2333426, GALEX J194138.5-233342) has $K_M = 16.3$, EPIC 217280630 (GALEX J191534.6-205107) has $K_M = 16.3$, EPIC 218366972 (2MASS 19345376-1855522, GALEX J193453.7-185552) has $K_M = 15.9$, and EPIC 218717602 (2MASS 19334689-1817137, GALEX J193346.9-181713) has $K_M = 15.8$.

These four stars were part of our K2 Guest Observer program which observed nine stars during C7, with these four pulsating. None of these stars were previously known to pulsate, making them new discoveries.

In §4 we will discuss how these stars fit with what has been learned from Kepler and published TESS (Transiting Exoplanet Survey Satellite Ricker et al. 2016) data to date with a brief review. As this is our 47th paper using Kepler data, and with recent TESS publications by Charpinet et al. (2019); Reed et al. (2020), and Sahoo et al. (2020), it is a good time to take an updated examination of group properties.

2 SPECTROSCOPIC OBSERVATIONS AND RESULTS

As part of our follow-up spectroscopic survey (Telting et al. 2014), low-resolution spectra ($R \sim 2000$) have been collected

for EPIC 215776487, EPIC 217280630, EPIC 218366972, and EPIC 218717602 using the 2.56m Nordic Optical Telescope (NOT) with ALFOSC, grism #18 and a 0.5 arcsec slit. We used CCD#14 giving an approximate wavelength range of 3450 – 5350Å, and a resolution based on the width of arc lines of 2.2Å. Exposure times of 900 s were used for all spectra.

The spectra were reduced and analyzed in the same way. Standard reduction steps within IRAF include bias subtraction, removal of pixel-to-pixel sensitivity variations, optimal spectral extraction, and wavelength calibration based on helium arc-lamp spectra. The target spectra and the mid-exposure times were shifted to the barycentric frame of the solar system. Radial velocities (RVs) were derived with the FXCOR package in IRAF. The RVs were adjusted for the position of the target in the slit, judged from slit images taken just before and after the spectral exposure.

The spectra of all four targets have the characteristic appearance of single sdB stars, for which we cannot exclude binarity with companions of much lower luminosity, such as main-sequence M stars or white dwarfs. For EPIC 217280630 no 2MASS magnitudes are listed. For the other 3 targets there is no clear near infrared excess observed (from 2MASS), again indicating single stars. Nevertheless, for EPIC 218366972 we detect clear RV variability (see below).

2.1 EPIC 215776487, EPIC 217280630, and EPIC 218717602

For EPIC 215776487, EPIC 217280630, and EPIC 218717602, we determined the RV with the average spectrum of each target as a template spectrum. We also used those average spectra to derive the atmospheric parameters of the stars, and we list these parameters in Table 1. For this purpose we used the fitting procedure of Edelman et al. (2003) with the metal-line blanketed local thermodynamic equilibrium (LTE) models of solar composition described in Heber et al. (2000).

For EPIC 215776487 we obtained nine useful spectra between Oct 2016 and Aug 2017, and achieved a signal-to-noise (S/N) level between 24 and 60 with median S/N=34. The average spectrum has S/N≈100. The median RV error is 8.4 km s⁻¹ and the RV root-mean-square (RMS) of the individual spectra around the average velocity is 7.1 km s⁻¹.

For EPIC 217280630 we obtained 10 useful spectra between Jun 2016 and Aug 2017, and achieved a S/N level between 29 and 57 depending on observing conditions, with median S/N=46. The average spectrum has S/N≈110. The median RV error is 9.9 km s⁻¹ and the RV RMS of the individual spectra around the average velocity is 10.5 km s⁻¹.

For EPIC 218717602 we obtained eight useful spectra between Oct 2016 and Aug 2017, and achieved a S/N level between 44 and 74, with median S/N=68. The average spectrum has S/N≈150. The median RV error is 5.3 km s⁻¹ and the RV RMS of the individual spectra around the average velocity is 7.8 km s⁻¹.

We conclude that for these three targets our RV measurements are consistent with single stars.

2.2 The orbit of EPIC 218366972

For EPIC 218366972 we obtained 12 useful spectra between Oct 2016 and Oct 2017, and achieved a S/N level between 34 and 71, with a median S/N=51. The average spectrum

Table 1. Results of spectral analysis. Errors on the final digits are given in parentheses.

Star	T_{eff} (K)	$\log g$ (cgs)	$\log \left(\frac{N_{\text{He}}}{N_{\text{H}}} \right)$
EPIC 215776487	27860(160)	5.45(2)	-2.718(38)
EPIC 217280630	22770(150)	5.01(2)	-2.104(77)
EPIC 218366972	28160(110)	5.44(2)	-2.862(28)
EPIC 218717602	24470(160)	5.17(2)	-2.633(61)

Table 2. Results of spectral binary analysis for EPIC 218366972.

Solution of RV wrt mean spectrum	
Amplitude	$64.01 \pm 3.09 \text{ km s}^{-1}$
Period	$5.9190 \pm 0.0021 \text{ d}$
Reduced χ^2	1.408
RMS	8.8 km s^{-1}
Solution of RV wrt model template	
System velocity	$38.12 \pm 3.51 \text{ km s}^{-1}$
Amplitude	$66.28 \pm 3.43 \text{ km s}^{-1}$
Period	$5.9218 \pm 0.0026 \text{ d}$
Reduced χ^2	0.73
RMS	8.8 km s^{-1}
Solution of RV wrt model template, with all RV errors set to 9.7 km s^{-1}	
System velocity	$38.20 \pm 3.15 \text{ km s}^{-1}$
Amplitude	$70.95 \pm 4.03 \text{ km s}^{-1}$
Period	$5.9187 \pm 0.0024 \text{ d}$
Reduced χ^2	1.00
RMS	7.9 km s^{-1}

has $S/N \approx 140$. For determining the RVs we have first used the average spectrum as a cross-correlation template, and subsequently a spectral model (as in Table 2) as a template. The median RV error is 7.7 km s^{-1} .

We find significant RV variations, and list the orbital solution obtained while assuming a circular orbit, in Table 2. With an orbital-velocity amplitude of 66.3 km s^{-1} , an orbital period of 5.92 days, and assuming that the companion is an unseen white dwarf, we derive the following constraints from the mass function. For a canonical mass of the subdwarf of $0.47 M_{\odot}$ (Van Grootel et al. 2014) the minimum mass of the WD companion is $0.58 M_{\odot}$. For an ensemble of a canonical-mass sdB with a canonical-mass WD ($0.6 M_{\odot}$) the orbital inclination is 79° . Assuming a mass of $0.3 M_{\odot}$ for the sdB the minimum mass of the WD is still $0.48 M_{\odot}$, and the minimum orbital separation is $12.6 R_{\odot}$. Using canonical masses and $i = 90^{\circ}$, the separation is $14.3 R_{\odot}$. At that separation and using $R_{\text{sdB}} = 0.2 R_{\odot}$, eclipses would occur for $i > 89^{\circ}$. No eclipses are observed in the K2 data (§3.3) indicating $i < 89^{\circ}$.

To determine the atmospheric parameters of EPIC 218366972, we shifted all individual spectra to remove the orbital velocities, and made an average orbit-corrected spectrum, to which we applied the same modelling procedure as described above for the other stars. The fit results are presented in Table 1.

3 K2 OBSERVATIONS AND PULSATION ANALYSES

Campaign 7 spanned 82 days between 4 October and 26 December, 2015. Our data are short-cadence observations,

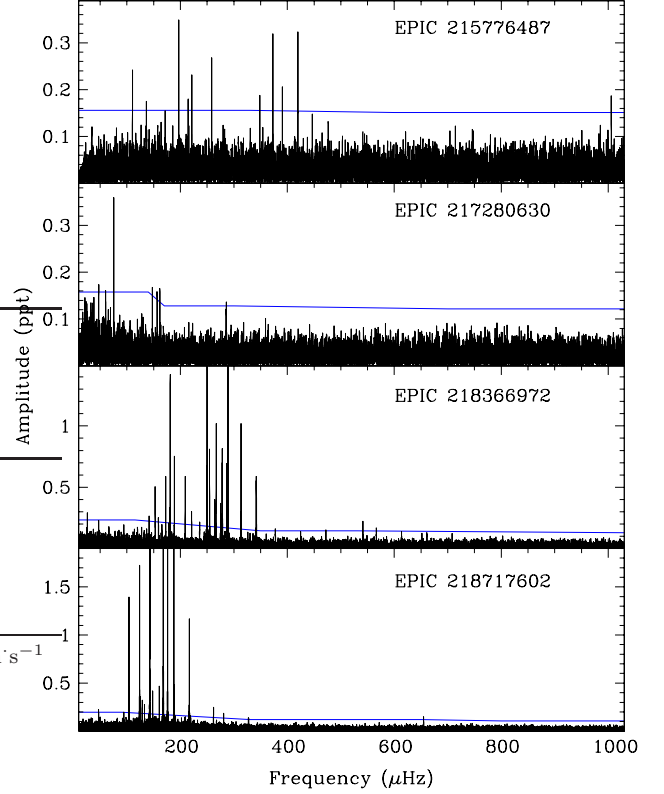


Figure 1. Fourier transforms of EPIC 215776487, EPIC 217280630, EPIC 218366972, and EPIC 218717602. Horizontal (blue on-line) lines indicate the detection threshold.

with integration times of 58.85 seconds which were downloaded from MAST as pixel files. Fluxes were extracted using aperture photometry and spacecraft artefacts were removed using our custom process described in Baran et al. (2017); Ketzner et al. (2017). Temporal spectra (Fourier transforms, FTs; Fig. 1) were produced to examine the pulsations and sliding FTs (SFTs) were produced to examine the time-stability of the pulsations. The $1.5/T$ frequency resolution of these data is $2.14 \mu\text{Hz}$ and to make it unlikely any peak in the FT is due to random noise requires a S/N of 4.2σ , where σ is the average level of the FT. As low frequency noise is more difficult to remove, σ were calculated in frequency regions nearly devoid of pulsations and linearly interpolated between, where pulsations occur.

Three of the four stars are exclusively g mode pulsators with only EPIC 218717602 having two p-mode periodicities. Most of the pulsations were amplitude and phase stable, in which case we prewhitened them using non-linear least-squares (nlls) fitting (e.g. Reed et al. 2004). Otherwise, we either Lorentzian fitted the FTs, using the Lorentzian widths as an estimator of frequency uncertainty only (e.g. Reed et al. 2014) or prewhitened smaller sections of data when the pulsations were significantly above the noise. Pulsations we detected are supplied in Tables 3 through 6. When the amplitudes were sufficiently stable for prewhitening, we include the fitting error in the tables, otherwise we do not.

While C7 spanned 82 days, to detect rotationally-split fre-

Table 3. Period list for EPIC 215776487. †: This frequency was fitted using data from days 25-40 of the run only with $\sigma = 0.086$ ppt.

ID	Freq μHz	Per Sec	Amp ppt	S/N	ℓ	n	$\frac{\Delta P}{P}$ %
f1	110.384 (8)	9059.31 (67)	0.27 (3)	7.3	1	33	3.2
f2	136.606 (10)	7320.30 (51)	0.23 (3)	6.3	1	26	0.03
f3	171.452 (13)	5832.53 (46)	0.16 (3)	4.4	1	20	-1.6
f4	197.027 (6)	5075.45 (16)	0.35 (3)	9.8	1/2	17/32	-7.7/-5.3
f5	214.565 (10)	4660.59 (22)	0.22 (3)	6.2	2	29	4.2
f6	221.276 (10)	4519.24 (21)	0.22 (3)	6.2	2	28	5.1
f7	258.647 (8)	3866.28 (12)	0.27 (3)	7.6	1	12	3.3
f8	348.718 (12)	2867.65 (10)	0.19 (3)	5.3	1	8	-0.5
f9	372.872 (7)	2681.88 (5)	0.32 (3)	9.0			
f10	390.700 (11)	2559.51 (7)	0.20 (3)	5.7	1		
f11	419.783 (7)	2382.18 (4)	0.32 (3)	9.0	1/2	6/13	3.2/8.4
f12†	1005.921 (71)	994.11 (7)	0.41 (7)	4.8			

Table 4. Period list for EPIC 217280630. † Values for f6 are from Lorentzian fitting.

ID	Freq μHz	Per Sec	Amp ppt	S/N	ℓ	n	$\frac{\Delta P}{P}$ %
f1	60.259 (8)	16549.39 (2.18)	0.144 (23)	6.2	1	80	-3.7
sA	65.295 (12)	15315.08 (2.81)	0.140 (22)	3.9	1	70	1.1
f2	75.454 (62)	13253.04 (10.84)	0.390 (22)	11.0	1	63	6.6
f3	147.652 (65)	6772.68 (2.96)	0.184 (22)	7.1	–	–	–
f4	156.544 (47)	6387.98 (1.91)	0.178 (22)	6.1	1	28	-4.3
f5	161.638 (54)	6186.66 (2.06)	0.153 (22)	5.9	1	27	-1.4
f6†	285.85 (18)	3498.31 (2.23)	0.107	–	1	13	2.7

quency multiplets usually requires two rotations within the observations. For stars where we do not detect frequency multiplets, we presume a spin period > 45 days. Of the 18 K1-observed sdBV stars, which had multiple years of data, eight (44%) had spin periods ≥ 45 days.

3.1 Pulsation analyses of EPIC 215776487

A total of 12 periodicities were detected above the detection threshold (shown as a horizontal blue line in Fig. 1) between 110 and 1006 μHz (994 and 9058 s). These were all stable in amplitude/frequency and so were nlls fitted. Their frequencies, periods, amplitudes, and S/N are provided in Tab. 3.

For g modes in sdB stars, typical $\ell = 1$ asymptotic period sequences have been found to have spacings ($\Pi_{\ell=1}$) near 250 s, and even a cursory differencing of EPIC 215776487's periods reveals similar spacings. In usual fashion, we do a Kolmogorov-Smirnov (KS) test, which can reveal commonly spaced periods. Very surprisingly for EPIC 215776487 there is no signature trough near 250 s to indicate the sequence (left panel of Fig. 2). Another tool used to discover asymptotic period sequences is an echelle diagram. We produced one with a spacing of 250 s and the sequence appeared (middle panel of Fig. 2). Using that as our guide, we found eight periods that are part of the $\ell = 1$ sequence and these modes indicate a period spacing of 247.3 ± 0.4 s. From the $\ell = 1$ sequence, an $\ell = 2$ sequence can be calculated from the relation $\Delta\Pi_{\ell=2} = \Delta\Pi_{\ell=1}/\sqrt{3}$. Two periods were found to fit the $\ell = 2$ sequence and two of the $\ell = 1$ periods could also fit the $\ell = 2$ sequence, and are marked accordingly in Tab. 3. All but two of the frequencies fit these sequences. f9 does not fit either sequence, though it is one of the highest-amplitude periodic-

ities. Perhaps this is a trapped mode, though we cannot confirm this as our series are not contiguous in n , which would be a necessary condition for finding trapped modes. There are no evenly-split frequencies indicative of rotationally-split multiplets and so we cannot determine a rotation period for EPIC 215776487. It is likely longer than our sensitivity, which is about 45 d.

3.2 Pulsation analyses of EPIC 217280630

We only detect six frequencies in EPIC 217280630's data set and two of these are very low near 60 and 75 μHz , which must be very close to the acoustic cut-off. All except for f6 were nlls fitted. A KS test has a significant trough just past 200 s and the echelle diagram confirms that sequence (both shown in Fig. 3). An additional low-amplitude peak (labeled sA in Tab. 4, which is obvious in the FT, below the detection threshold, but fits the asymptotic sequence is included in both the figure and the table for EPIC 217280630. Linear regression determines $\Pi_{\ell=1} = 207.56 \pm 0.26$ s for EPIC 217280630, with only f3 not fitting the $\ell = 1$ sequence. Like EPIC 215776487, this non-sequence periodicity has a fairly high amplitude (the second highest) and so could represent a trapped $\ell = 1$ mode, though we have no way to confirm this. The sequence has only one contiguous pair, and so there is no way to search for trapped modes. The period spacing of 207 s is extreme for a cool (coolest of these four stars), purely-g-mode pulsator. There are two other sdBV stars with small $\Pi_{\ell=1}$ values, but they are much hotter, p+g hybrid pulsators. There are no indicators of rotationally-induced frequency multiplets which we interpret as a long (> 45 d) rotation period. However, it could also indicate an orientation

Table 5. Period list for EPIC 218366972. † frequencies were Lorentzian fitted. * indicates mode identifications which are less certain.

ID	Freq μHz	Per Sec	Amp ppt	S/N	ℓ	n	$\frac{\Delta P}{P}$ %
sA	119.945 (10)	8337.14 (71)	0.203 (26)	4.0	1/2	29/53	-0.5 / -6.0
sB	127.638 (11)	7834.66 (66)	0.191 (26)	3.8	1	27	2.8
sC	136.773 (11)	7311.39 (61)	0.183 (26)	3.7	1/2	25/46	-2.1 / -2.9
f04	141.552 (07)	7064.53 (37)	0.297 (28)	5.9	1	24	1.3
f05	152.926 (4)	6539.13 (17)	0.548 (28)	11.3	1	22	-4.4
f06	159.091 (8)	6285.72 (32)	0.267 (28)	5.8	1/2	21/39	-3.6 / 0.3
sD	165.698 (10)	6035.08 (37)	0.126 (28)	4.0	1	20	-1.7
f08	172.580 (4)	5794.43 (12)	0.591 (28)	12.5	1	19	4.1
f09	178.679 (10)	5596.61 (30)	0.212 (28)	4.5			
f10	181.005 (2)	5524.70 (5)	1.398 (28)	29.6	1	18	-1.5
f11	188.826 (3)	5295.88 (8)	0.766 (26)	16.2			
f12	209.051 (3)	4783.53 (8)	0.597 (26)	13.2	1	15	8.4
f13	221.076 (7)	4523.34 (14)	0.309 (26)	6.8	1/2	14/27	6.5 / 3.0
f14	236.030 (8)	4236.75 (15)	0.252 (26)	5.8	1/2	13/25	-5.7 / -8.3
f15†	244.74 (23)	4086.1 (3.8)	0.16 (-)	-	2	24	5.0
f16	249.782 (1)	4003.48 (1)	2.742 (26)	62.3	1	12	3.0
f17	254.659 (2)	3926.82 (4)	0.832 (26)	18.9	2	23	-2.2
f18	264.374 (5)	3782.51 (7)	0.439 (26)	18.9	2	22	-0.2
f19	267.029 (2)	3744.92 (3)	1.020 (28)	10.0	1	11	1.8
f20	275.184 (6)	3633.94 (8)	0.370 (28)	23.2	2	21	-1.2
f21	278.242 (4)	3593.99 (5)	0.637 (28)	14.4			
f22	278.543 (3)	3590.10 (4)	0.769 (28)	17.5			
f23†	283.21 (26)	3531.0 (3.2)	0.13 (-)	-			
f24	286.534 (3)	3489.98 (4)	0.743 (28)	18.1	1/2	10/20	-2.0 / 1.0
f26	289.181 (1)	3458.04 (2)	1.538 (28)	37.5	1	10	-10.5
f27	313.565 (2)	3189.14 (2)	1.023 (28)	25.8	1/2	9/18	-0.3 / -3.4
sE	326.205 (12)	3065.56 (12)	0.168 (26)	4.3	*2	17	12.7
f29	330.446 (12)	3026.21 (11)	0.177 (26)	4.6	*2	17	-14.1
f30	341.948 (4)	2924.42 (3)	0.452 (28)	11.6	1	8	1.1
f31	342.134 (5)	2922.83 (4)	0.489 (28)	12.5	1	8	0.5
sF	360.526 (16)	2773.73 (12)	0.129 (26)	3.9			
f33	377.650 (10)	2647.95 (7)	0.188 (25)	6.0	1	7	-1.9
f34	424.882 (13)	2353.59 (7)	0.151 (25)	4.5			
f35	472.046 (12)	2118.44 (5)	0.165 (25)	5.2	1	5	0.9
f36	541.427 (9)	1846.97 (3)	0.241 (26)	7.2	1	4	-0.3
sG	613.733 (13)	1629.37 (4)	0.146 (25)	3.9			
sH	651.577 (12)	1534.74 (3)	0.164 (25)	3.9			
sI	660.887 (16)	1513.12 (4)	0.137 (25)	4.3			
sJ	661.036 (17)	1512.78 (4)	0.111 (25)	4.0			
sK	708.144 (12)	1412.14 (2)	0.158 (25)	4.1			

where the $m \neq 0$ components are of lower amplitude, and therefore undetected.

3.3 Pulsation analyses of EPIC 218366972

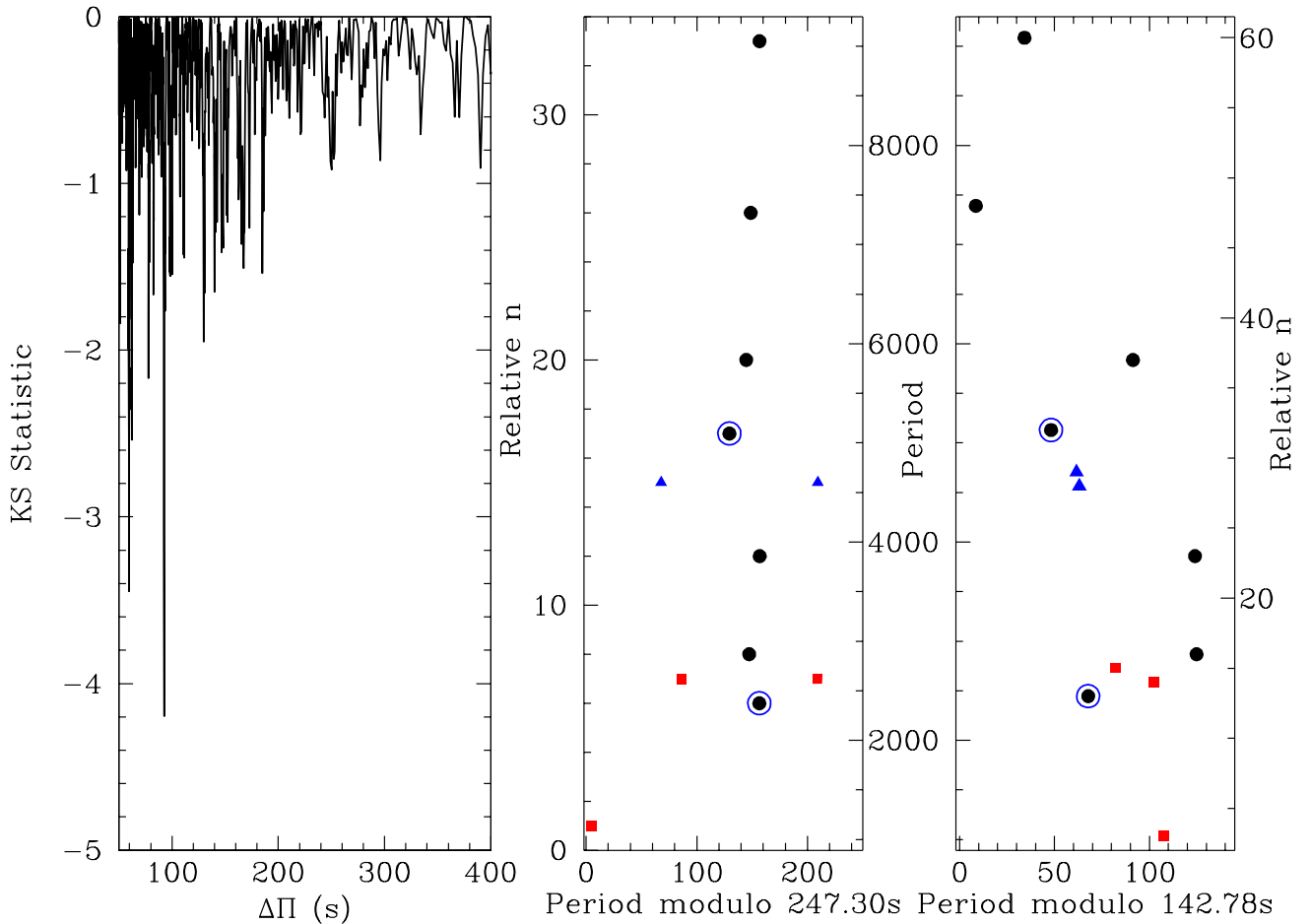
EPIC 218366972 is the richest pulsator of the group. We detect 36 periodicities above the detection limit with another 11 *suspected*. The strongest trough in the KS test (left panel of Fig. 4) is near 250 s, though it is not especially significant compared to others. As $\ell = 1$ modes have the least geometric cancellation (Pesnell 1985) and therefore typically higher amplitudes, we did an amplitude cut at 0.5 ppt and, with just those periods, the trough became significant. The echelle diagram (right panel of Fig. 4), spaced at 254 s, easily shows that sequence, however EPIC 218366972 has a significant “hook” feature at lower radial overtones. This has been seen in several other sdBV stars (Baran & Winans 2012). We calculated a period spacing of 254.95 ± 0.50 s with linear regression above the hook, and then linearly fitted the hook feature for inclu-

sion in Tab. 5. We calculated where $\ell = 2$ sequence periodicities should occur from the $\ell = 1$ sequence and those that match are labelled as such in Tab. 5. Many of the $\ell = 1$ modes also match the $\ell = 2$ sequence, and since we cannot distinguish between them, we label them with both. An intriguing feature is how linear the periods look below the turn of the “hook” feature (< 4000 s). A KS test of just those periods reveals a broad peak with a central value of 271 s and folding across that period produces an echelle with seven periods in line. As such, an alternative view would be that there is a sequence with periods > 3450 s with an asymptotic spacing of 254.95 s and another at 271 s up to and including f26 (3458 s).

Surprisingly for so many frequencies there are no obvious rotationally-induced frequency multiplets. If EPIC 218366972 were tidally locked, a rotation period of 5.9 d would be a frequency of about $2.0 \mu\text{Hz}$ and $\ell = 1$ modes would have a separation of half that near $1.0 \mu\text{Hz}$. There are no frequency splittings near those values or multiples. The closest we find to a multiplet would be a possible triplet of f15-f16-f17, which

Table 6. Period list for EPIC 218717602. † f18 was nlls fitted using only the first 10 days of data with $\sigma = 0.07$ ppt.

ID	Freq μHz	Per Sec	Amp ppt	S/N	ℓ	n	$\frac{\Delta P}{P}$ %
f01	103.904 (2)	9624.29 (14)	1.376 (27)	40.5	1	33	0.1
f02	123.749 (1)	8080.89 (8)	1.689 (27)	49.7			
f03	124.653 (6)	8022.30 (40)	0.293 (27)	8.6	1	27	-8.7
f04	128.692 (6)	7770.48 (39)	0.371 (27)	11.0	1	26	-4.4
f05	132.902 (8)	7524.35 (41)	0.264 (27)	7.8	1/2	25/46	2.1/-4.7
f06	142.845 (1)	7000.58 (4)	2.400 (28)	70.6	1	23	3.0
f07	143.045 (1)	6990.82 (6)	1.760 (28)	51.8	1	23	-0.7
f08	148.202 (5)	6747.56 (22)	0.431 (27)	12.7	1	22	6.9
f09	160.668 (5)	6224.03 (18)	0.451 (27)	13.4	1	20	7.9
f10	168.133 (1)	5947.67 (2)	3.710 (27)	112.4	1	19	2.9
f11	176.074 (1)	5679.44 (3)	1.989 (27)	60.3	1	18	1.0
f12	187.938 (1)	5320.91 (3)	2.127 (27)	64.5			
f13	216.857 (2)	4611.33 (4)	1.121 (27)	35.0	1	14	-4.9
f14	261.915 (9)	3818.03 (14)	0.227 (27)	7.1	1	11	-6.4
f15	280.983 (9)	3558.93 (15)	0.169 (27)	5.4	1	10	-4.9
f16	327.077 (11)	3057.39 (10)	0.129 (18)	4.8	1	8	4.5
f17	327.867 (10)	3050.02 (10)	0.135 (18)	5.0	1	8	1.7
f18†	7876.05 (14)	126.967 (2)	0.368	5.3			
f19	8110.90 (7)	123.290 (1)	0.122 (43)	4.5			

**Figure 2.** KS test (left panel) and echelle diagrams (right two panels) for $\ell = 1$ and 2 asymptotic sequences of EPIC 215776487, respectively. In the echelle diagrams, black circles indicate periods that match the $\ell = 1$ sequence, blue triangles match the $\ell = 2$ sequence, black circles with a blue surround match both sequences, and red points do not fit either sequence.

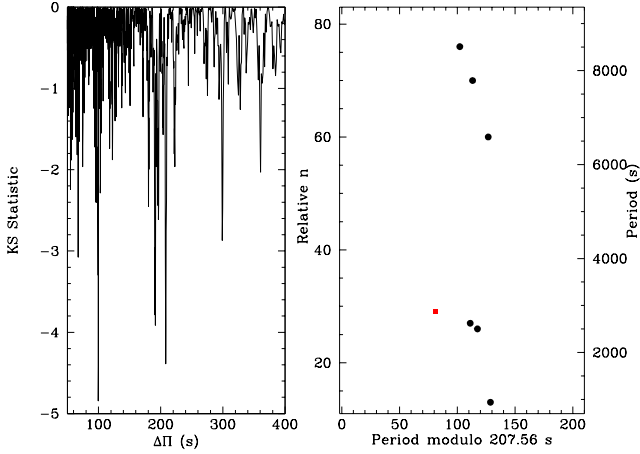


Figure 3. KS test (left panel) and $\ell = 1$ echelle diagram (right panel) for EPIC 217280630. Point shapes and colours (on-line only) as in Fig. 2.

are split by 4.95 and 4.88 μHz , respectively. However, those three periods also fit asymptotic sequences, making that a more likely fit. As such, we do not detect any frequency multiplets in EPIC 218366972. In this case, binarity indicates an orientation favorable for viewing multiplets, and so we can safely assume that the rotation period is > 45 d.

We can also use the FT to search for a signal from Doppler boosting caused by the binary motion. Following the method of [Telting et al. \(2012\)](#) and using $K = 67 \text{ km}\cdot\text{s}^{-1}$, we calculate a Doppler boosting signal of 0.3 ppt at 1.96 μHz . The final step in our lightcurve processing removes trends > 1.5 days, and so we examined a lightcurve without this processing step. Unfortunately, the unprocessed lightcurve has low-frequency noise greater than 0.3 ppt and so we cannot detect the binary signal using Doppler boosting. There is also no indication of eclipses in the lightcurve.

3.4 Pulsation Analyses of EPIC 218717602

We were able to prewhiten 19 frequencies for EPIC 218717602 and, as is obvious just by looking at the FT, most of these readily fit into an $\ell = 1$ asymptotic sequence. The KS test shows a very deep trough near 265 s, which is easily reproduced in the echelle diagram (both are shown in Fig. 5). There is a slight hook feature, but a linear regression finds a period spacing of 263.15 ± 0.48 s. This sequence includes all but four of the g modes. Of those, there are two pairs (f02, f03 & f16, f17) separated by $0.84 \pm 0.08 \mu\text{Hz}$. If $\ell = 1$ (as f03, f16, and f17 fit the sequence) then this would be a rotation period of about 7 d. These are not the highest amplitude pulsations in EPIC 218717602 and so the multiplet detection is not secure. EPIC 218717602 also has two p-mode frequencies, with f18 only appearing at the beginning of the run. However, without any observational evidence for mode identifications, they do not tell us much. Only that another quite cool sdB star has p modes (see Tab. 7 for others).

4 EXAMINING THE GROUP

Kepler’s original mission (K1) observed 18 sdBV stars ([Østensen et al. 2010, 2011](#)) and K2 observed 139 of our proposed sdB targets in short-cadence mode during its 20 campaigns. Many K1-observed sdBV stars have over three years, or about 1.5 million data points, of observations, while K2 only observed individual fields for roughly 80 days, resulting in about 110 000 data points per target. While this vast wealth of data takes quite some time to process (particularly K2 stars for which we have to begin with pixel files), first-look analyses anticipates about 50 pulsators from K2. To date a total of 34 of the roughly 69 Kepler-observed sdBV stars have been analyzed and published (including the four in this paper), so there is still some ways to go. Additionally, TESS has now completed its two year main mission, during which it observed about 1 000 of our proposed sdB targets, few of which have been examined as of this writing. As such, it seems a good point to examine progress and compare and review what has been detected.

Thanks to a generous time allocation from the NOT, we have been able to obtain spectra of all of our Kepler targets ([Telting et al. 2014](#)). We do this both to constrain binarity and so that we are fitting the same resolution spectra to the same atmospheric model grids. While there may be systematics between model grids or differing instrumentation in data from multiple sources, our single-sourced *relative* values should be accurate. We refer readers to any of the references provided in Tab. 7 for details on the spectra and their processing. Table 7 lists seismic, spectroscopic, and orbit-rotation properties of 38 published (or *in press*) Kepler-observed sdBV stars, one blue horizontal branch (BHB) star with closely related pulsation properties, and four TESS-observed sdBV stars. Rotation is deduced strictly from pulsation frequency multiplets while the binary period may be deduced from RV or photometric variations. To date, from K1 there were two stars analyzed for which multiplets were not detected while K2 has many. From K1, we know that rotation periods typically span tens of days, and so any periods longer than about 45 d (44% of K1 stars) would not likely be resolved during K2 observations. Each TESS sector of observations spans about 26 days, and so rotation periods longer than about 12 days (68% of K1+K2 stars) would likely not be detected. In this “group” summary, we only consider sdBV stars observed during K1, K2, and TESS missions and excluding atypical pulsation types (e.g. [Jeffery et al. 2017](#)). This sample should include stars with similar bulk physical properties that have observations obtained in a roughly-homogeneous manner capable of providing mode identifications. Two exceptions to this are the sdB+WD binaries Feige 48 ([Reed et al. 2012](#)) and KPD 1930+2752 ([Reed et al. 2011](#)) included only in Fig. 11 which have binary periods under one day and rotation periods derived from ground-based pulsation data.

The real revolution from Kepler data is the ability to observationally correlate periodicities with pulsation modes (mode identifications). The main tools which have been used are asymptotic g-mode period spacings, which provide ℓ and relative n values; rotationally-induced frequency multiplets, which provide ℓ , m , and can provide relative n if several multiplets of the same degree are detected; and g-mode frequency multiplets splittings, which have relative spacings dictated by

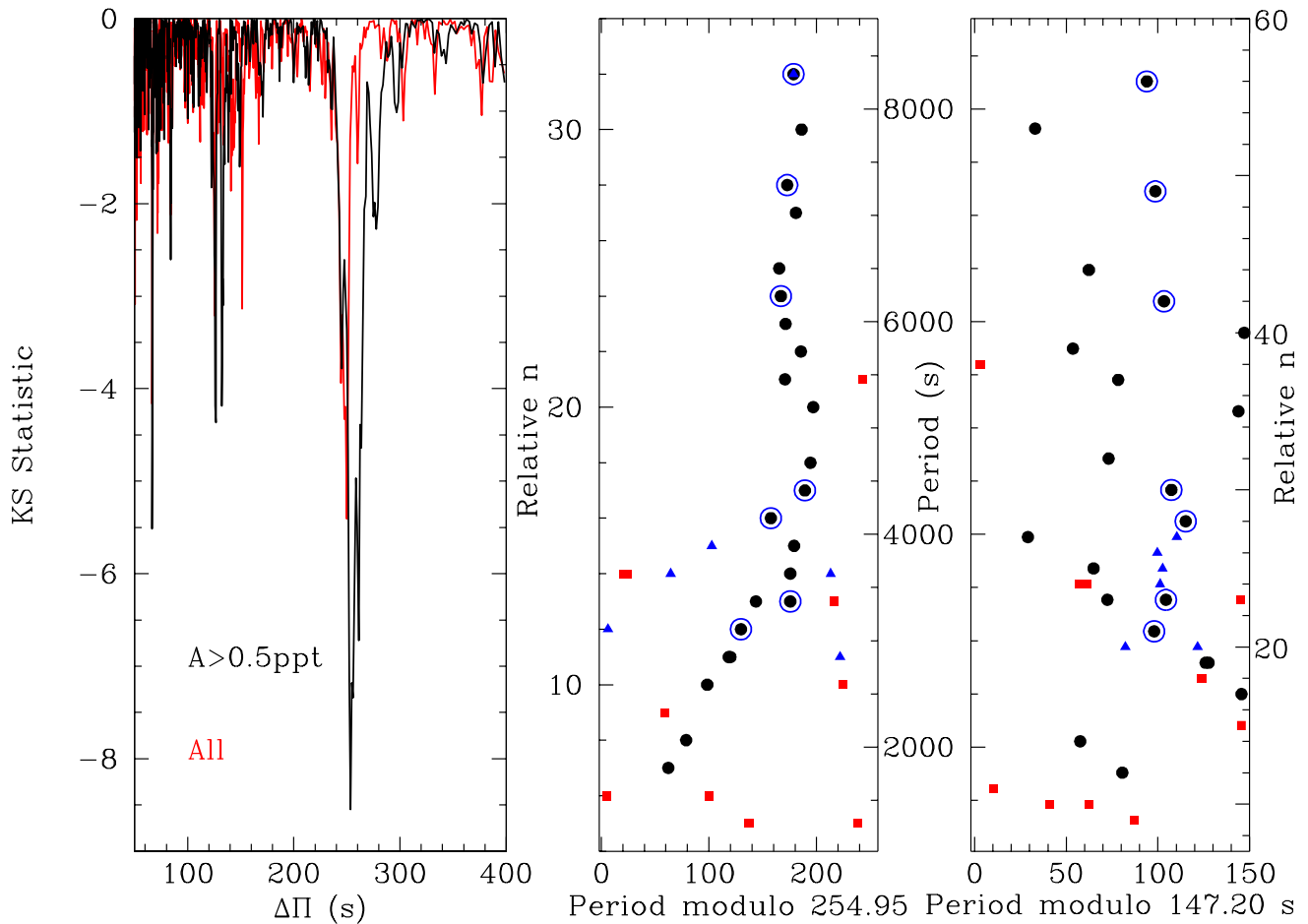


Figure 4. Same as Fig. 3 for EPIC 218366972.

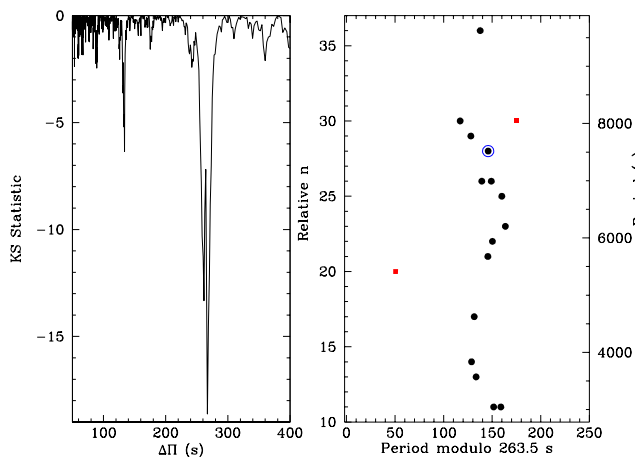


Figure 5. Same as Fig. 3 for EPIC 218717602.

the Ledoux constant (Ledoux 1951), and this can provide ℓ values.

These identifications are invaluable for constraining stellar structure models, from which we discern inter-

nal physics. Important pulsation properties include the smoothness of asymptotic sequences (e.g. Reed et al. 2014), which describe less stratified transition regions than expected (Constantino et al. 2015); mode trapping (e.g. Østensen et al. 2014), which has now been associated with convective core overshoot (Guo & Li 2018; Ostrowski et al. 2021); both p and g mode overtone spacings (Reed et al. 2011; Baran et al. 2012), which describe the resonant cavity; and frequency multiplets, which provide information on rotation, including differential rotation, and for stars in binaries, which all indicate subsynchronous rotation for close binaries (periods under 10 days, e.g. Telting et al. 2012), with the exception of the 3 hour binary 2M1938+4603 (Østensen et al. 2010), constraining synchronization time scales for post-common-envelope (PCE) binaries (e.g. Pablo et al. 2012). Hybrid pulsators allow for radial scrutiny as g modes probe deeper than p modes (Charpinet et al. 2014), with the latter being mostly envelope (defined as above the He/H transition).

Figure 6 shows the locations of the pulsators in Table 7 in a Kiel diagram. Included in the figure are non-pulsators observed during K1 (Østensen et al. 2010, 2011) and sample zero-age helium main-sequence (ZAEHB) and evolutionary tracks (Reed et al. 2004). It is well-known that a larger fraction of sdB stars are observed to pulsate in g modes than

p modes, or equivalently, cooler sdB stars are more likely to pulsate at observable amplitudes than hotter ones. Therefore it is not too surprising that most of the Kepler-observed stars are g+p. Commensurate with that is very few of the non-pulsators observed by Kepler are cooler sdB stars. There is only one below 26 000 K while above 30 000 K 26 of the 28 (93%) K1-observed stars are not observed to pulsate.

4.1 Hybrid pulsators

While models have largely been successful in predicting where p-mode pulsations should occur in the Kiel diagram (contours in Fig. 7), there has been difficulty getting g-mode instabilities up to observed effective temperatures (Jeffery & Saio 2006a,b; Hu et al. 2009; Bloemen et al. 2014). Prior to Kepler observations, it was presumed that p-mode pulsations occurred in hotter sdB stars, g-mode pulsations occurred in cooler sdB stars, and rare hybrid pulsators would inhabit the temperature boundary. However, as can be seen in Figs. 6 and 7, hybrid pulsators occur across nearly the full range of temperatures, including the hottest and third coolest stars in our sample. In Tab. 7 the transition from p+g to g+p occurs at 29 000–30 000 K. The coolest p+g star and the hottest g+p star both have $T_{\text{eff}} = 29\,600\text{ K}$.

4.2 Pulsators in binaries

Table 7 separates the pulsators by binary type. All of our sdB binaries with white dwarf or M-dwarf companions are g+p, though we know this is not a unique feature. Ground-based observations have observed p mode sdBV stars with both types of companions. All save one of our Kepler/TESS-observed sdBV stars with F/G companions are p+g pulsators. That sole g+p pulsator (CD–28° 1974), observed with TESS, is also the hottest g+p star. Perhaps these trends are indicative of formation channels, as the sdB+WD/dM binaries would have experienced at least one common-envelope (CE) phase (Han et al. 2002, 2003) while the sdB+F/G binaries would likely have had their envelopes stripped via Roche-lobe-overflow (RLOF) (e.g. Vos et al. 2017). There could also be an observational bias in that cooler sdB stars are fainter than their F/G companions, making them harder to detect. This could likely be answered by examining our full set (K1, K2, and TESS) of non-pulsators which were initially selected using GALEX observations. If there were a reasonable number of GALEX-selected sdB stars below 30 000 K with F/G companions, then we can rule out an observational selection effect. This should be revealed in our forthcoming K2 summary paper when pulsators and non-pulsators are compared.

Slightly more than half of our pulsators show no indication of a companion. This means there were no indications of spectral lines from a companion, no RV variations outside of standard deviations, and no photometric variations which could be produced by the reflection effect, ellipsoidal variations, Doppler boosting, or phase-induced pulsation aliasing caused by light-travel across an orbit. SdB formation channels include stripping giant stars at the tip of the red giant branch via RLOF or CE ejection, or by merging two helium white dwarfs (WDs). The result of the different evolutionary paths is that the envelope-stripping ones produce sdB stars with masses sharply peaked at the so-called “canonical”

value of $0.47M_{\odot}$ or slightly less while merged WDs can have a broad range of masses from 0.4 to over $0.7M_{\odot}$ (See Fig. 12 of Han et al. 2003). GAIA data should help answer this question as it will detect astrometric binaries and, in many cases, determine masses when combined with spectroscopic and/or spectral energy distribution data.

4.3 Observational correlations and trends

Observations are meant to provide constraints and direction to models, from which we determine the physics of stars. Observations we list in Table 7 include spectroscopic ones, T_{eff} , $\log g$ and binarity, and seismic ones, pulsation type, P_{Amax} (period of highest amplitude), $\Pi_{\ell=1}$ (g-mode asymptotic period spacing for $\ell = 1$), and rotation period (from frequency multiplets).

Figure 8 is a Kiel diagram where point colours indicate detected $\Pi_{\ell=1}$. There are no obvious trends. The longer period spacings are mostly clustered in the middle (around $T_{\text{eff}} = 27\,000\text{ K}$ and $\log g = 5.35$), the median values (near $\Pi_{\ell=1} = 250 - 260\text{ s}$) extend from $T_{\text{eff}} = 23\,000\text{ K}$ to $T_{\text{eff}} = 30\,000\text{ K}$, and the lower period spacings have tendencies to be towards the extremes; $\log g > 5.5$ or $T_{\text{eff}} < 27\,000\text{ K}$, which also includes lower $\log g$. Clearly asymptotic period spacings depend on something other than temperature or gravity.

Figure 9 shows the period of the highest-amplitude pulsation (P_{Amax}) in each star with T_{eff} . Point type and colour indicate binary information. As previously noted, the sdB+F/G binaries are in the hottest group of stars. The p+g-mode pulsators show P_{Amax} for both types of pulsations, connected by dotted lines. Even though the log scale compresses the ordinate, there is a clear trend of P_{Amax} towards longer periods in cooler stars. This trend seems clear in the g/g+p region but less so in the p/p+g stars. If we ignore the sdB+F/G stars, the p mode periods show a clear trend in the same direction as the g modes, whereas if we include those, there is little correlation and even a slightly reversed trend.

4.4 Rotation

It was pointed out in Reed et al. (2014) that there was a trend for cooler stars to have longer rotation periods. With more pulsators studied, this is re-examined in Fig. 10. There are four differential rotators (indicated by points joined by a line) and K2 and TESS data often did not detect multiplets, which means either the pulsations are pole-on, or we only have a lower limit on rotation. We presume the latter, as shown by arrows in Fig. 10, as pole-on orientations are unlikely. Two exceptions may be K10001893 and K8302197 for which no multiplets were detected in over 1 000 days of K1 data, indicating either a pole-on viewing angle, or extremely slow rotation (> 715 days). Open points in Fig. 10 indicate rotation was determined from p-mode multiplets. It has been observed that in radially differential rotators (Foster et al. 2015, and below) p modes indicate faster rotation than g modes. Rather than a correlation, we can now only state that below 24 000 K rotation is only slower than 45 days and above 32 500 K rotation is only faster than 25 days. There are no binary stars in our sample cooler than 26 000 K and no sdB+dM or sdB+WD binaries hotter than 32 000 K.

The effect of binarity on rotation is investigated in Fig. 11.

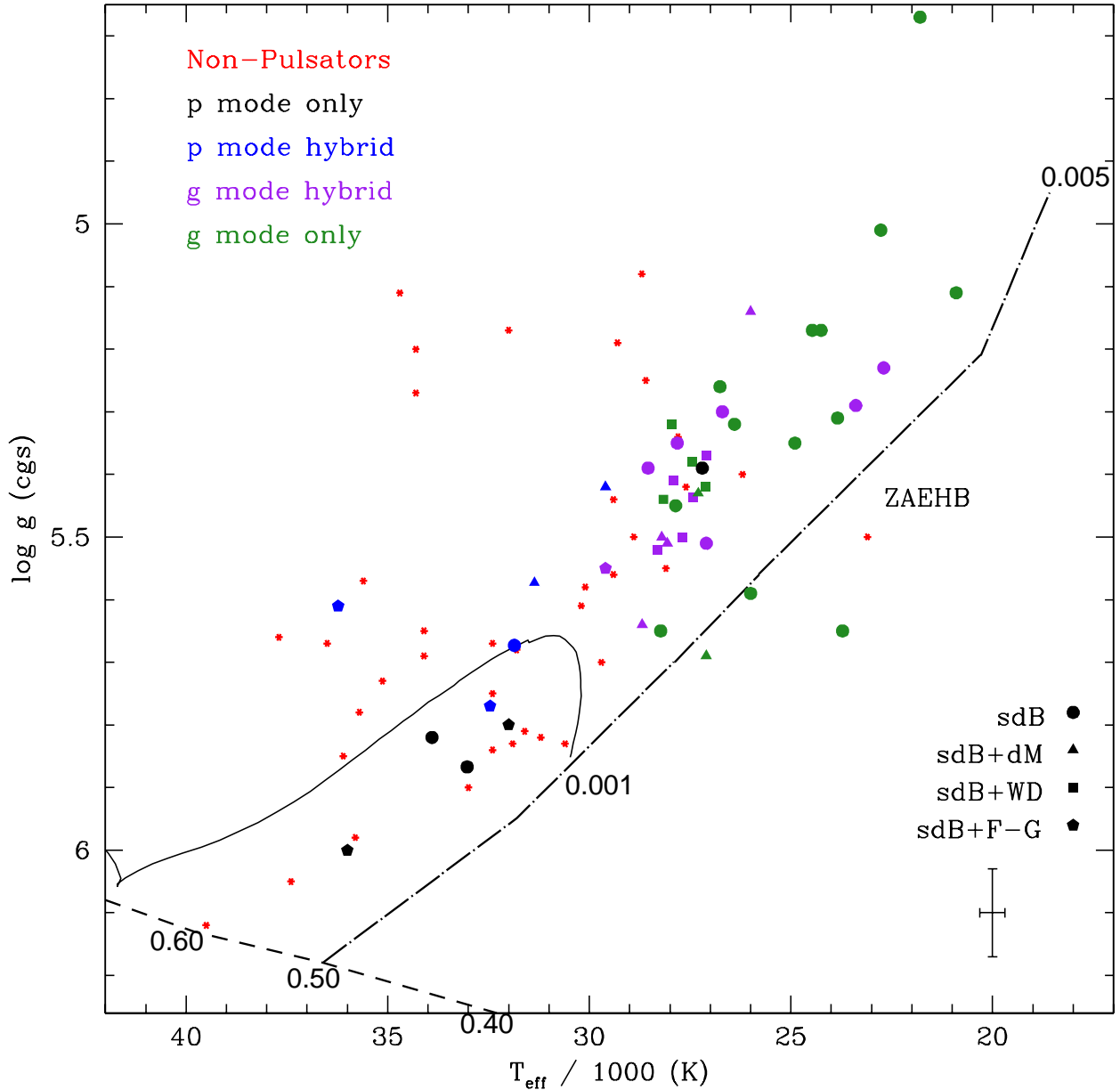


Figure 6. Kiel diagram of Kepler and TESS-observed sdB stars. Colours and symbols are indicated within the figure: Non-pulsators are not shaped for binary information. The dashed-dotted line indicates the zero-age helium main-sequence (ZAEHB) for a core mass of $0.50M_{\odot}$ with varying envelope masses (two are labeled on the plot) and the dashed line indicates the ZAEHB for a fixed envelope mass of $2 \times 10^{-4}M_{\odot}$ and varying core masses (three are labeled on the plot). The solid lines show evolution for a core mass of $0.001M_{\odot}$ and an envelope mass of $0.001M_{\odot}$. Errorbars for the average of the errors from Table 7 are indicated in the lower right.

The black diagonal line indicates tidally-locked rotation. Interesting features in Fig. 11 include that *all* space-based-observed sdB+WD stars are primarily g-mode pulsators that rotate subsynchronously. As there are only eight such systems, and g-mode pulsations occur more often than p-mode ones, this may be a selection effect. We include the two p-mode sdB+WD stars Feige 48 (Reed et al. 2012) and KPD 1930+2752 (Reed et al. 2011) (from ground-based data)

as they are the shortest-period sdB+WD binaries which also have frequency multiplets to indicate rotation period. KPD 1930+2752 is tidally locked while Feige 48 is nearly so. All the g-mode sdB+WD binaries have very similar rotation periods, though four of those only have lower limits on rotation. The sdB+dM binaries all have short binary periods, and this is almost certainly a selection effect. They are usually detected by the so-called “reflection effect” where the

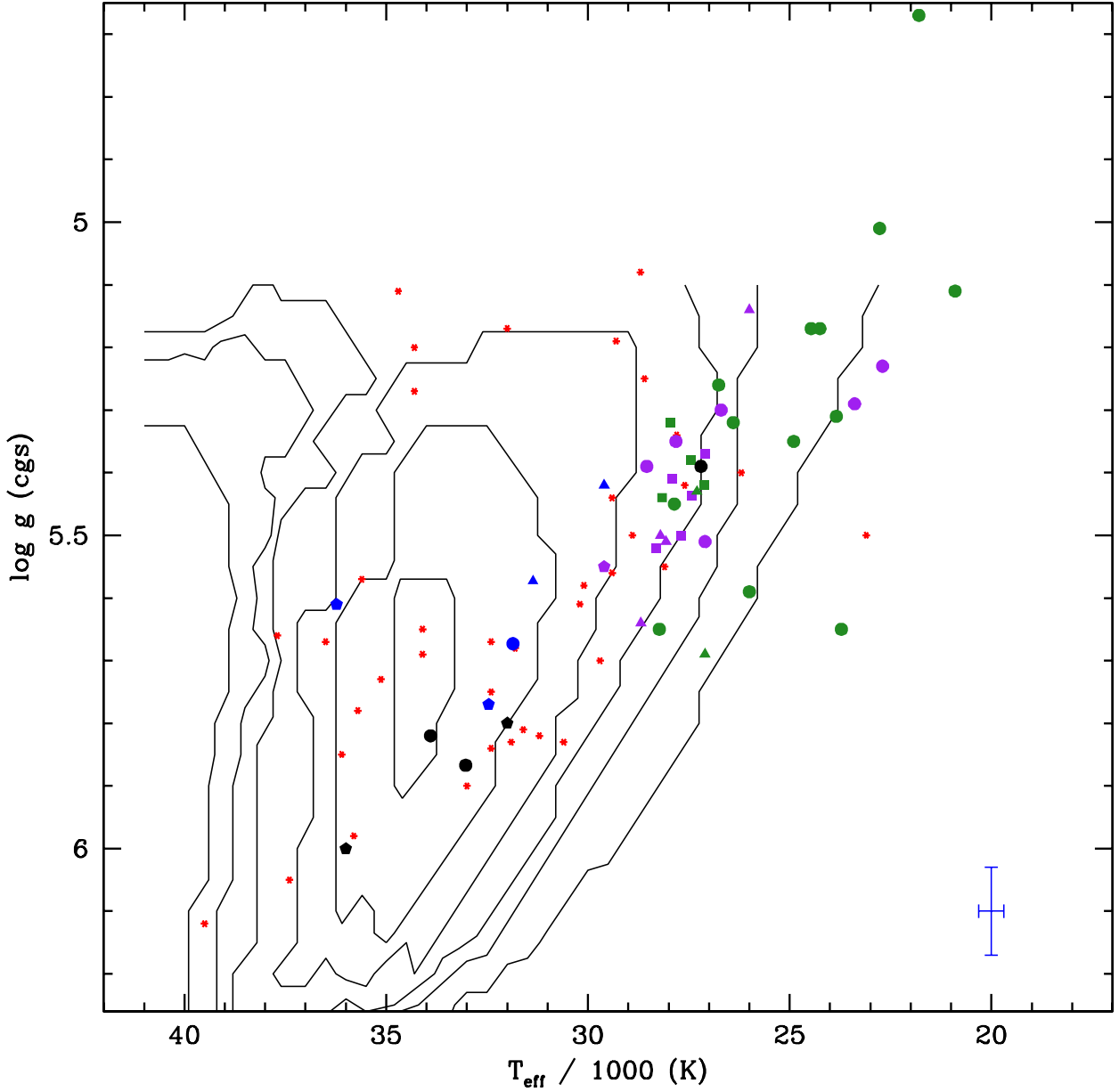


Figure 7. Kiel diagram showing p-mode instability contours (reproduced from [Charpinet et al. 2001](#)) with points and average errorbars from [Figure 6](#).

sdB stars heat one side of the dM stars, causing brightness variations with the orbital period. This effect will not be detected if the binary separation is too large and the dM will not be observed as the sdB star far outshines it (e.g. §3 of [Reed & Stiening 2004](#)). The sdB+dM binaries in our sample are tidally locked until the binary period exceeds ~ 0.25 d then they all rotate subsynchronously. The sdB+F/G stars in our sample rotate commensurate with their apparently single sdB counterparts in the same temperature range ([Fig. 10](#)) but supersynchronous to their long-period orbits.

[Figure 12](#) shows the eight stars where multiplets have been

detected in both p and g modes, or there were sufficient pulsations that they should have been, providing a lower limit. It is expected that p-mode pulsations mostly sample the envelope while g-mode pulsations sample deeper into the star ([Charpinet et al. 2014](#)). To date there have been five that appear to be radially-differential rotators ([Baran et al. 2017](#); [Foster et al. 2015](#); [Reed et al. 2019, 2020](#); [Baran et al. 2019](#)) and three that likely rotate as solid-bodies ([Baran et al. 2012](#); [Kern et al. 2017](#); [Reed et al. 2019](#)). There are no obvious correlations with binarity as half of the apparently single and sdB+F/G stars rotate differentially and half rotate like solid

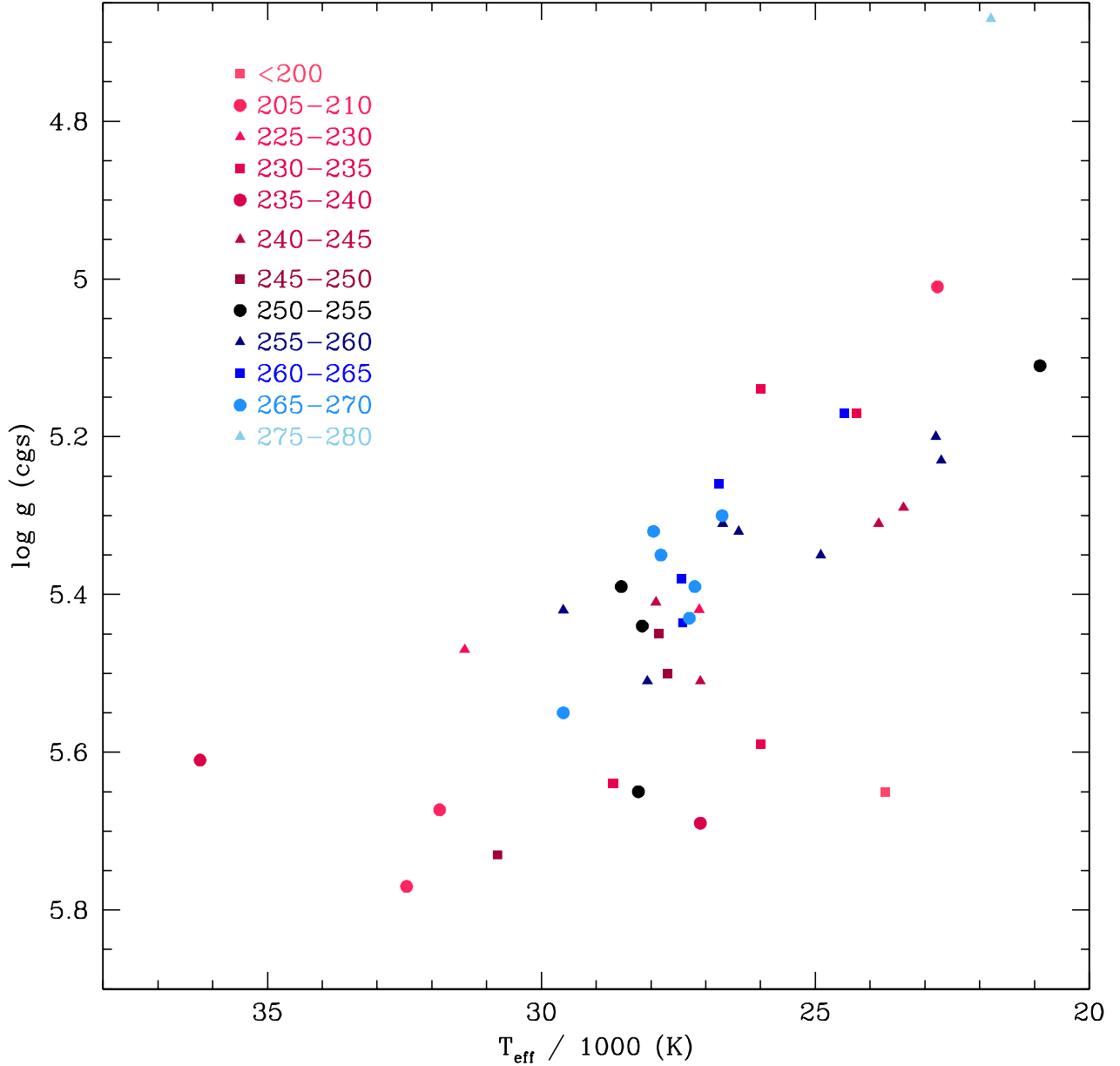


Figure 8. Kiel diagram showing $\ell = 1$ g-mode period spacings, $\Pi_{\ell=1}$. Colour codings provided in the figure and different point types are for clarity only.

bodies. Both of the sdB stars with dM companions rotate differentially. In all cases of differential rotation, p-mode pulsations indicate faster rotation than g-mode pulsations, with the possible exception of KIC 10139564 (Baran et al. 2012) which has 1σ errorbars that overlap the solid-body rotation line.

5 DISCUSSION

5.1 Campaign 7 Pulsators

In this paper we analyzed four newly-discovered sdBV stars and add them to the growing number of sdBV stars with a large fraction of identified pulsation modes. We detect asymptotic g-mode period spacing sequences in all four, with three having $\Pi_{\ell=1}$ values right near 250 s and the other near to 200 s. Only three other sdBV stars have such unusually short asymptotic spacings; two are hot p+g pulsators and the other another cool g-mode-only pulsator. So the extremely low

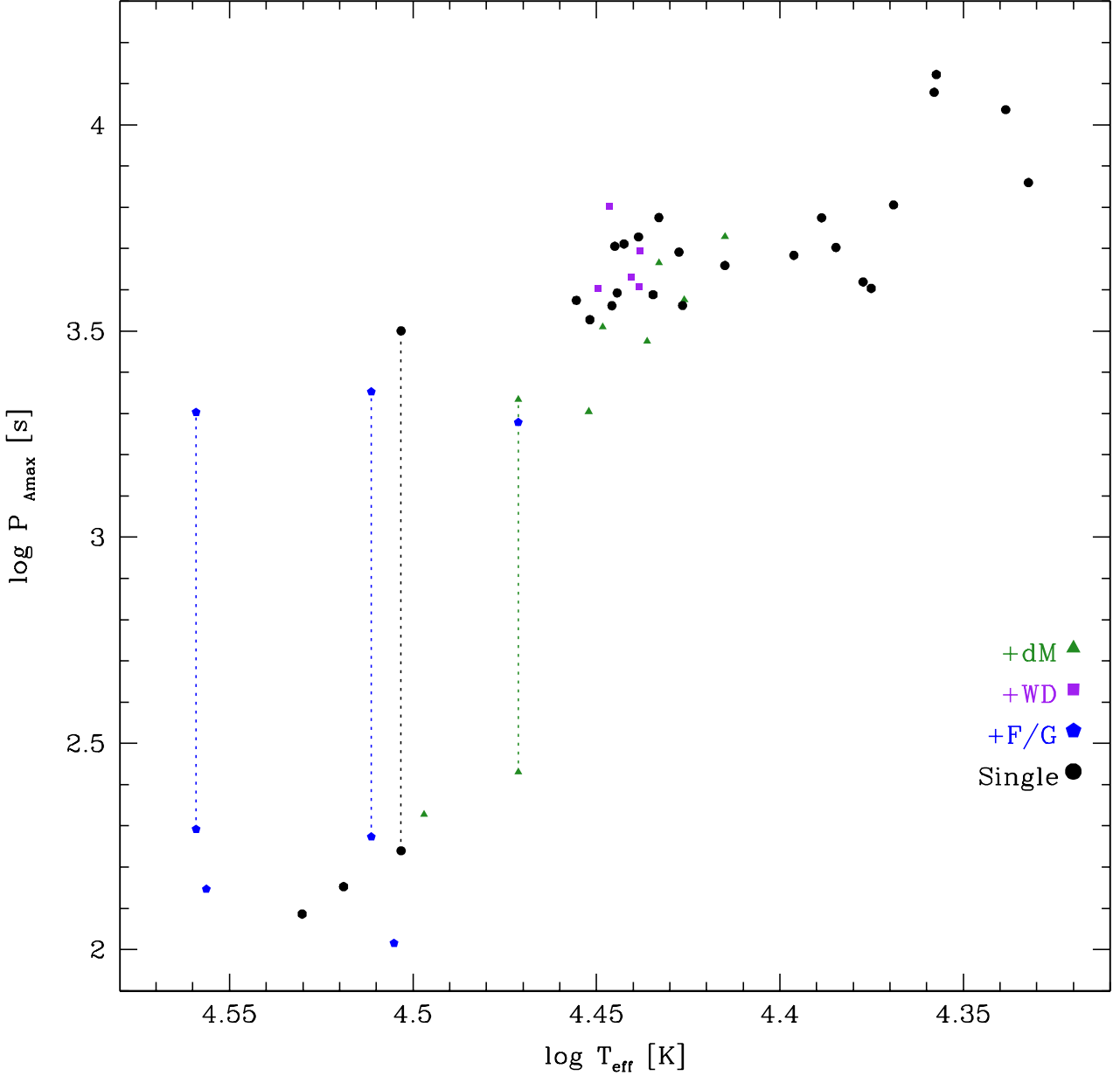


Figure 9. Comparing T_{eff} to P_{Amax} . The four p+g pulsators have their g-mode P_{Amax} connected to their p-mode P_{Amax} by dotted lines. Note that CD-28° 1974 has had its point shifted down 0.02 dex for clarity. Point shapes and colours (on-line only) are indicated in the figure.

asymptotic spacings only occur for stars at both extremes. However, stars with similar physical properties to each group also have “normal” spacings near to 250 s and so this mystery has yet to be solved.

Three of the stars in C7 are apparently single, while we have discovered EPIC 218366972 to have RV variations, indicative of a white dwarf companion in a 5.92 d orbit. Somewhat surprisingly we do not detect any multiplets in EPIC 218366972 and so presume the rotation period to be > 45 d. Only in EPIC 218717602 do we detect multiplets

which indicate a rotation period near 7 d. We could have anticipated detecting two sdBV stars with multiplets based on the 56% detection rate from K1 for periods under 45 days.

5.2 The Group of Kepler and TESS-observed Pulsating Subdwarf B Stars

We completed ensemble analyses so that modelers may use this information to deduce physical processes within these stars. In our analyses we have only included Kepler and

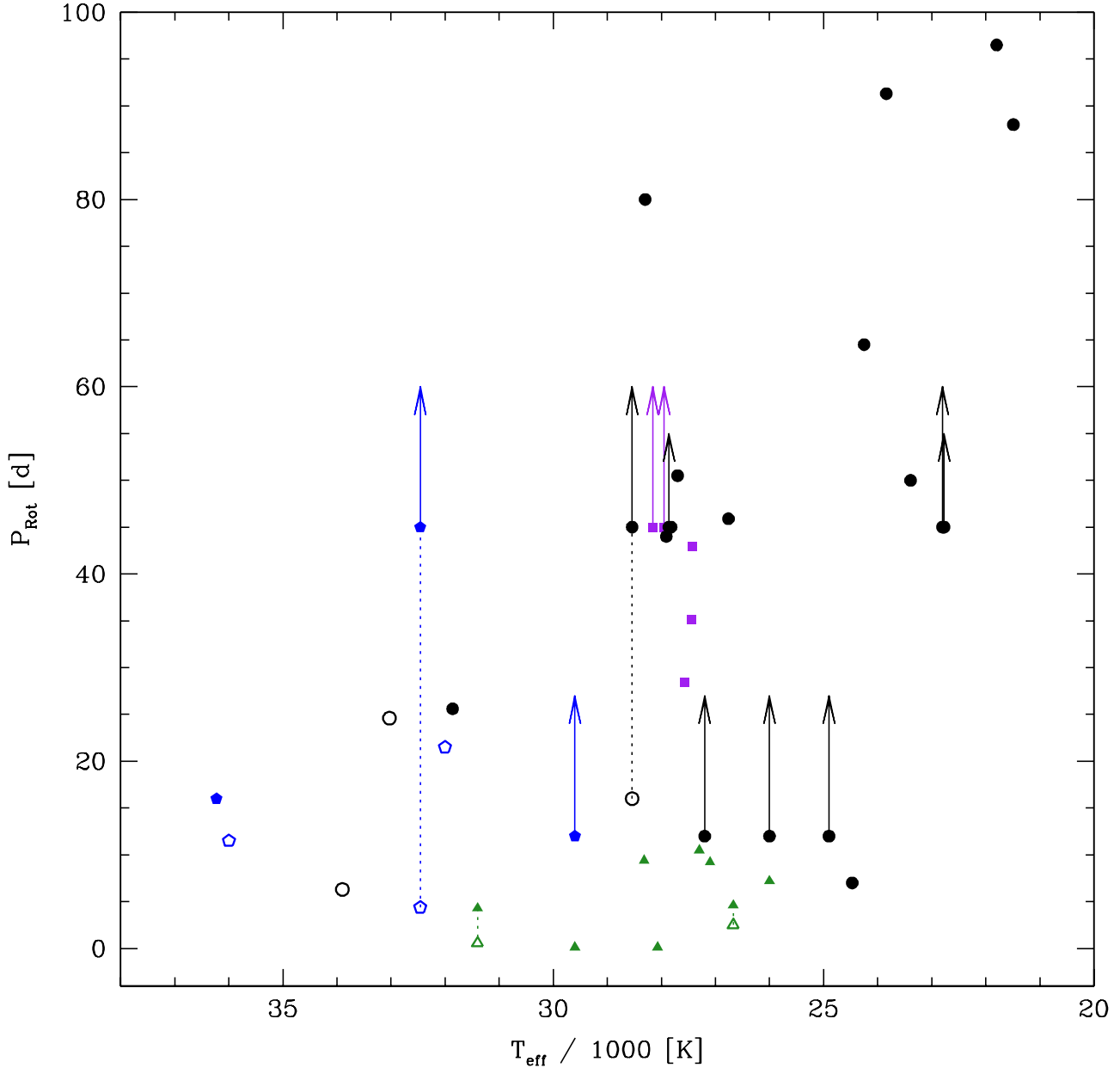


Figure 10. Comparing T_{eff} to rotation periods. Arrows indicate lower limits and dotted lines connect rotation periods that are different for p and g modes. Open symbols indicate rotation was determined from p-mode multiplets. Point shapes and colours (on-line only) are the same as Fig. 9.

TESS-observed sdBV stars as it provides a roughly homogeneous observing sample with the highest quality data. In examining the group, we think we have revealed some underlying relationships which may prove fruitful for model study.

5.2.1 Pulsations

As has been known for some time, pulsators and non-pulsators overlap in the Kiel diagram (Figs. 6 and 7), with a higher percentage of cool sdBV stars pulsating with g modes.

It has been observed that hotter stars favour p modes and cooler ones favour g modes, and we also find this. Of the 43 stars in our sample, the dividing line between p+g and g+p pulsators is 29 000-30 000 K. The p/p+g pulsators cluster around the central instability contour indicating that pulsation driving models are likely reasonably accurate. Driving models for g-mode pulsations have been less certain (which is why instability contours are not included in Fig. 7) as the temperature range seems strongly dependent on the amount of enhancement of iron-group elements in the driving region

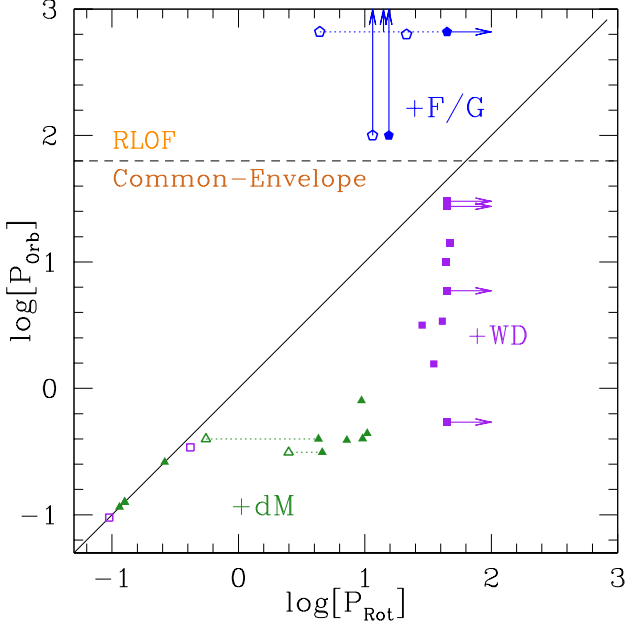


Figure 11. Comparing orbital to rotation periods. Arrows indicate lower limits and dotted lines connect rotation periods that are different for p and g modes. Open points indicate rotation was determined from p-mode multiplets. Point shapes and colours (on-line only) are the same as Fig. 9. Diagonal line indicates tidally-locked rotation. The figure includes the sdB+WD binaries Feige 48 (Reed et al. 2012) and KPD 1930+2752 (Reed et al. 2011) which have periods less than one day even though neither was observed by Kepler. We also include the sdB+dM binary AADor which is not a pulsator but has a spectroscopically determined rotation period (Vuckovic et al. 2016).

(e.g. Jeffery & Saio 2006b; Hu et al. 2009). More problematic are the hybrid pulsators. Originally discovered in a limited mid-temperature range bordering p and g pulsations, Kepler and TESS observations detect them from 22 800 to 36 300 K. 49% of the stars in our sample are hybrid pulsators. Pulsation driving models will need to account for the two hybrids with p modes completely outside those instability contours and g-mode pulsations that span from 22 800 to 36 300 K.

Our sample has seven stars (16%) with T_{eff} below 25 000 K and none are in known binaries. Similarly there are no PCE (sdB+WD/dM) binaries with T_{eff} above 31 500 K in our sample (also seven stars), though at least two are known from ground-based observations; the sdB+dM binary PG 1336-018 (Kilkenny et al. 1998) and the sdB+WD binary KPD 1930+2752 (Billères et al. 2000). This poses two questions; Does binarity shut off pulsation driving below 25 000 K? And does PCE binarity adversely effect pulsation driving above 31 500 K? It is likely too early to draw conclusions (particularly on the hot side, where two systems are known) but this will be worth watching as the sample is completed for K2-discovered pulsators and increased with TESS data.

Of the relationships we examined, the one with the clearest correlation appears to be between T_{eff} and P_{Amax} which shows a clear trend for cooler stars to have longer periods (lower frequencies) of their highest-amplitude pulsations. Reed et al. (2020) noted two g-mode outliers below the trend that both have indications of smaller-than-canonical masses.

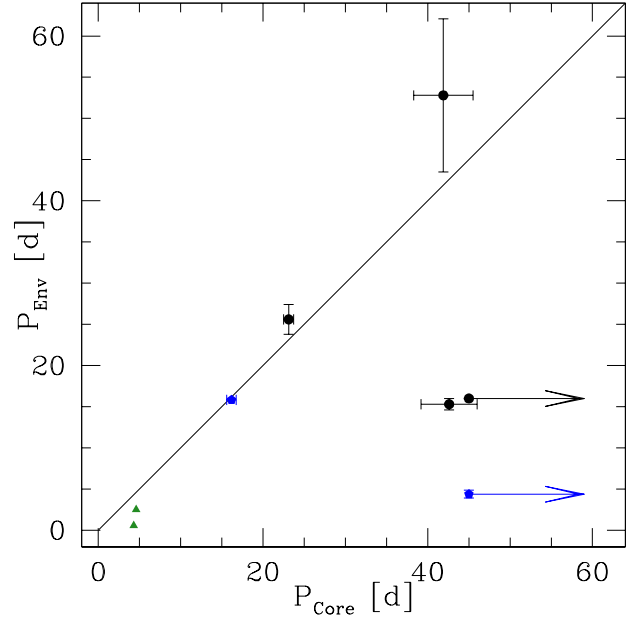


Figure 12. Comparing envelope to interior rotation periods for stars where multiplets have been detected in both g and p modes. PG 0048 and E211779126 only have lower limits for their g-mode pulsations. Errorbars are omitted when smaller than the points. Point shapes and colours (on-line only) are the same as Fig. 9.

If the $T_{\text{eff}}-P_{\text{Amax}}$ relationship is indicative of the resonant cavity size, then stars along this relationship would likely have a common convective core size (inner boundary of the resonant cavity) with varying envelope thicknesses. Thicker envelopes equate to lower T_{eff} , a larger resonant cavity, and therefore longer P_{Amax} . Another outlier (E248368658) above the trend could indicate a higher-massed core.

Related to the $T_{\text{eff}}-P_{\text{Amax}}$ relationship, we anticipated finding a similar relationship with mean period spacings, $\Pi_{\ell=1}$, but do not. A recent study by Uzundag et al. (2021) examined $\Pi_{\ell=1}$ in models with a narrow range of total mass and two convective core masses. They note that $\Pi_{\ell=1} \propto \bar{g}^{-1} R_*/(R_* - R_{\text{core}})$. From this, they found agreement with previous studies (e.g. Castellani et al. 1985; Constantino et al. 2015; Ostrowski et al. 2021), that smaller convective cores have smaller $\Pi_{\ell=1}$ and stars with larger convective cores, and consequently lower $\log g$, have larger $\Pi_{\ell=1}$. Those results could be indicative of why Fig. 8 shows no obvious patterns.

5.2.2 Rotation

We examined the correlation between rotation period and T_{eff} (Fig. 10), as noted by Reed et al. (2014), and find that it only seems to hold at extreme values of T_{eff} . In our sample there are no fast-rotating cool nor slowly-rotating hot sdBV stars with no known binaries at all in our cool sample and no PCE (sdB+WD/dM) binaries in our hot sample. The mid- T_{eff} star E217280630 has a rotation period of 7 days which is in a range dominated by sdB+WD binaries. It would be worth obtaining additional observations to search for a white dwarf companion.

Unfortunately there is currently little hope for additional constraints on those stars with only lower limits on their rotation periods. No ground-based observations have resolved multiplets in g-modes of sdBV stars and transparency variations, which occur on similar time scales to those pulsation periods, make it extremely difficult even to observe g-mode sdBV pulsations without space-borne telescopes. As K1 observations show, only long-duration space-based observations are likely to fully resolve frequency multiplets and provide rotation periods.

Patterns do emerge when comparing orbital to rotation periods of known binary systems. First, all PCE stars in our sample with binary periods longer than 0.3 days rotate subsynchronously while those shorter than 0.3 days are synchronized.

All of our sdB+WD systems with measured rotation periods are between 28 and 51 days. There are two known sdB+WD systems with shorter binary periods and also rotation periods under one day (Fig 11). While 44% of our sample only have lower limits near 45 days, we would speculate that sdB+WD systems, which have undergone two common-envelope phases, have a common PCE initial rotation period near 45 days which then evolves towards shorter periods.

We see a very similar pattern in our sample of sdB+dM binaries. Four stars have periods near 10 days, three stars are tidally locked with periods under 0.3 days, and two are in between and differentially rotating with the envelope spinning faster. This has two possibilities; either the rotation of these binaries, which have only had one common-envelope epoch, is correlated with the binary period, or these PCE systems also have a common initial rotation period which evolves to shorter periods. We think the latter is the most likely explanation, particularly since the differential rotators have faster-spinning envelopes which are likely being spun up by the companions, through tidal interactions. Furthermore, the dissipation of tidal energy can be achieved in the form of pulsations.

Our sample of sdB+F/G stars are only on the hot end and rotate faster than the average but not dissimilar to single sdB stars in the same temperature range. It is presumed their temperatures are related to thinner envelopes yet material deeper within (g mode) sdB stars is correlated with slower rotation. As these stars likely formed via RLOF perhaps that mechanism produces faster rotators, or conversely, RLOF does not slow rotation during mass loss like the CE mechanism does. A larger sample of sdB+F/G stars may answer this question.

It is more difficult to find meaning with differential rotation (Fig. 12). Both of the sdB stars with dM companions for which we have both p and g-mode multiplets have differential rotation. It is unlikely a common property of all sdB stars with dM companions as two sdB stars with dM companions in Fig. 11 have g-mode multiplets indicating they are tidally locked. As all the sdB+dM rotation periods are short, TESS data will likely expand this sample. Our sample of sdB+F/G stars and those without known companions shows a mixture. We would encourage investigations to determine if any of these systems have short-period companions, as difficult as that may be. Only by ruling out binarity with periods up to ten days can we determine if differential rotation is inherent to a property unrelated to binarity. If it is not related to binarity, then a companion “spinning up” sdB stars cannot be

the cause and it must therefore be related to mass loss near the tip of the red giant branch.

The above relationships likely relate to mass loss and angular momentum transport during their formation mechanisms. Another piece of evidence is the comparison between binary and rotation periods. Most PCE sdB stars in our sample rotate subsynchronously to their orbit unless it is less than about half a day. This information should be useful in modeling PCE binaries.

5.3 The Future

Our examination of the group properties includes an intermediate sample from K2 and a very preliminary sample from TESS. There are over a dozen suspected pulsators observed during K2 which have yet to be thoroughly analyzed and TESS has now observed thousands of sdB stars, with perhaps a couple hundred new pulsators. Those data should produce a statistically significant sample from which to examine pulsation properties. However, even with an expanded sample, rotation is likely to be problematic as K1 showed us that we really need continuous data for more than a year before we are likely to resolve frequency multiplets.

We did not examine individual periods of the stars in our ensemble in our analyses. So in addition to the properties discussed in this paper, we encourage modelers to examine properties which include trapped modes, radial indices where asymptotic sequences begin and end, the “hook” feature in asymptotic sequences, and the standard deviation in Π (e.g. Constantino et al. 2015). Additionally, it may well be worth a look at other “hook”-feature pulsators to see if they too have a different linear asymptotic period sequence shortward of the bend, as EPIC 218366972 does.

Separate from pulsations, GAIA is providing reliable parallaxes (Bailer-Jones et al. 2018; Gaia Collaboration et al. 2021), from which distances, radii, and masses can be determined (e.g. Kilkeny et al. 2019; Baran et al. 2019; Reed et al. 2020). In combination with the remaining K2 sdBV stars, and the many yet to be discovered by TESS, powerful observational tools are becoming available. We are likely on the brink of understanding the underlying relationships hinted at in this paper.

Data Availability Statement: The data underlying this article are available in the Mikulski Archive for Space Telescopes (MAST). <https://archive.stsci.edu/> Data obtained with the Nordic Optical Telescope is available after a one-year proprietary period. <http://www.not.iac.es/archive/>

ACKNOWLEDGMENTS: Funding for this research was provided by the National Science Foundation grant #1312869 and NASA grant 14-K2GO2-2-0047 as part of the K2 guest observer program. Any opinions, findings, and conclusions or recommendations expressed in this material are those of the authors and do not necessarily reflect the views of the National Science Foundation or NASA. JAC was funded by the Missouri Space Grant, which is funded by NASA. ASB gratefully acknowledges financial support from the Polish National Science Centre under projects No. UMO-2017/26/E/ST9/00703 and NOUMO-2017/25/B/ST9/02218. This paper includes data obtained by the *Kepler* mission. Funding for the *Kepler* mission is provided by the NASA Science Mission directorate. Data pre-

sented in this paper were obtained from the Mikulski Archive for Space Telescopes (MAST). STScI is operated by the Association of Universities for Research in Astronomy, Inc., under NASA contract NAS5-26555. Support for MAST for non-HST data is provided by the NASA Office of Space Science via grant NNX13AC07G and by other grants and contracts.

The spectroscopic observations used in this work were obtained with the Nordic Optical Telescope at the Observatorio del Roque de los Muchachos and operated jointly by Denmark, Finland, Iceland, Norway, and Sweden.

REFERENCES

- Bachulski S., Baran A. S., Jeffery C. S., Østensen R. H., Reed M. D., Telting J. H., Kuutma T., 2016, *Acta Astron.*, 66, 455
- Bailer-Jones C. A. L., Rybizki J., Fousneau M., Mantelet G., Andrae R., 2018, *AJ*, 156, 58
- Baran A., Telting J., Østensen R., Winiarski M., Drożdż M., Koziel D., Reed M., Oreiro R., Silvotti R., Siwak M., Heber U., Papis P., 2010, *Ap&SS*, 329, 199
- Baran A. S., Østensen R. H., Telting J. H., Vos J., Kilkenny D., Vuckovic M., Reed M. D., Silvotti R., Jeffery C. S., Parsons S. G., Dhillon V. S., Marsh T. R., 2018, *MNRAS*, 481, 2721
- Baran A. S., Reed M. D., Østensen R. H., Telting J. H., Jeffery C. S., 2017, *A&A*, 597, A95
- Baran A. S., Reed M. D., Stello D., Østensen R. H., Telting J. H., Pakštienė E., O’Toole S. J., Silvotti R., Degroote P., Bloemen S., Hu H., Van Grootel V., Clarke B. D., Van Cleve J., Thompson S. E., Kawaler S. D., 2012, *MNRAS*, 424, 2686
- Baran A. S., Telting J. H., Jeffery C. S., Østensen R. H., Vos J., Reed M. D., Vuckovic 2019, *MNRAS*, 489, 1556
- Baran A. S., Telting J. H., Németh P., Bachulski S., Krzesiński J., 2015, *A&A*, 573, A52
- Baran A. S., Telting J. H., Németh P., Østensen R. H., Reed M. D., Kiaeerad F., 2016, *A&A*, 585, A66
- Baran A. S., Winans A., 2012, *ActaAstron*, 62, 343
- Billères M., Fontaine G., Brassard P., Charpinet S., Liebert J., Saffer R. A., 2000, *ApJ*, 530, 441
- Bloemen S., Hu H., Aerts C., Dupret M. A., Østensen R. H., Degroote P., Müller-Ringat E., Rauch T., 2014, *A&A*, 569, A123
- Castellani V., Chieffi A., Tornambe A., Pulone L., 1985, *ApJ*, 296, 204
- Charpinet S., Brassard P., Fontaine G., Van Grootel V., Zong W., et al. 2019, *A&A*, 632, A90
- Charpinet S., Brassard P., Van Grootel V., Fontaine G., 2014, in van Grootel V., Green E., Fontaine G., Charpinet S., eds, 6th Meeting on Hot Subdwarf Stars and Related Objects Vol. 481 of *Astronomical Society of the Pacific Conference Series*, On Interpreting g-Mode Period Spacings in sdB Stars. p. 179
- Charpinet S., Fontaine G., Brassard P., 2001, *PASP*, 113, 775
- Charpinet S., Fontaine G., Brassard P., Green E. M., Van Grootel V., Randall S. K., Silvotti R., Baran A. S., Østensen R. H., Kawaler S. D., Telting J. H., 2011, *Nature*, 480, 496
- Constantino T., Campbell S., Christensen-Dalsgaard J., Lattanzio J., Stello D., 2015, *MNRAS*, 452, 123
- Edelmann H., Heber U., Hagen H.-J., Lemke M., Dreizler S., Napitowitzki R., Engels D., 2003, *A&A*, 400, 939
- Foster H. M., Reed M. D., Telting J. H., Østensen R. H., Baran A. S., 2015, *ApJ*, 805, 94
- Gaia Collaboration Brown A. G. A., Vallenari A., et al. 2021, *A&A*, 649, A1
- Green E. M., Fontaine G., Reed M. D., Callera K., Seitzzahl I. R., White B. A., Hyde E. A., Østensen R., Cordes O., Brassard P., Falter S., Jeffery E. J., Dreizler S., Schuh S. L., Giovannini M., Edelmann H., Rigby J., Bronowska A., 2003, *ApJL*, 583, L31
- Guo J.-J., Li Y., 2018, *MNRAS*, 478, 3290
- Han Z., Podsiadlowski P., Maxted P. F. L., Marsh T. R., 2003, *MNRAS*, 341, 669
- Han Z., Podsiadlowski P., Maxted P. F. L., Marsh T. R., Ivanova N., 2002, *MNRAS*, 336, 449
- Heber U., 2016, *PASP*, 128, 082001
- Heber U., Reid I. N., Werner K., 2000, *A&A*, 363, 198
- Howell S. B., Sobek C., Haas M., Still M., Barclay T., Mullally F., Troeltzsch J., Aigrain S., Bryson S. T., Caldwell D., Chaplin W. J., Cochran W. D., Huber D., Marcy G. W., Miglio A., Najita J. R., Smith M., Twicken J. D., Fortney J. J., 2014, *PASP*, 126, 398
- Hu H., Nelemans G., Aerts C., Dupret M., 2009, *A&A*, 508, 869
- Jeffery C. S., Baran A. S., Behara N. T., Kvammen A., Martin P., Naslim N., Østensen R. H., Preece H. P., Reed M. D., Telting J. H., Woolf V. M., 2017, *MNRAS*, 465, 3101
- Jeffery C. S., Saio H., 2006a, *MNRAS*, 371, 659
- Jeffery C. S., Saio H., 2006b, *MNRAS*, 372, L48
- Kern J. W., Reed M. D., Baran A. S., Østensen R. H., Telting J. H., 2017, *MNRAS*, 465, 1057
- Kern J. W., Reed M. D., Baran A. S., Telting J. H., Østensen R. H., 2018, *MNRAS*, 474, 4709
- Ketzer L., Reed M. D., Baran A. S., Németh P., Telting J. H., Østensen R. H., Jeffery C. S., 2017, *MNRAS*, 467, 461
- Kilkenny D., Koen C., O’Donoghue D., Stobie R. S., 1997, *MNRAS*, 285, 640
- Kilkenny D., O’Donoghue D., Koen C., Lynas-Gray A. E., van Wyk F., 1998, *MNRAS*, 296, 329
- Kilkenny D., Worters H. L., Lynas-Gray A. E., 2019, *MNRAS*, 485, 4330
- Ledoux P., 1951, *ApJ*, 114, 373
- Østensen R. H., Degroote P., Telting J. H., Vos J., Aerts C., Jeffery C. S., Green E. M., Reed M. D., Heber U., 2012, *ApJL*, 753, L17
- Østensen R. H., Green E. M., Bloemen S., Marsh T. R., Oreiro R., Laird J. B., Morris M., Moriyama E., Reed M. D., Kawaler S. D., Aerts C., Vuckovic M., Degroote P., Telting J. H., et al., 2010, *MNRAS*, 408, L51
- Østensen R. H., Reed M. D., Baran A. S., Telting J. H., 2014, *A&A*, 564, L14
- Østensen R. H., Silvotti R., Charpinet S., et al. 2010, *MNRAS*, 409, 1470
- Østensen R. H., Silvotti R., Charpinet S., et al. 2011, *MNRAS*, 414, 2860
- Østensen R. H., Telting J. H., Reed M. D., Baran A. S., Németh P., Kiaeerad F., 2014, *A&A*, 569, A15
- Ostrowski J., Baran A. S., Sanjayan S., Sahoo S. K., 2021, *MNRAS*, 503, 4646
- Pablo H., Kawaler S. D., Reed M. D., Bloemen S., Charpinet S., Hu H., Telting J., et al. 2012, *MNRAS*, 422, 1343
- Pesnell W. D., 1985, *ApJ*, 292, 238
- Randall S. K., Green E. M., Fontaine G., Brassard P., Terndrup D. M., Brown N., Fontaine M., Zacharias P., Chayer P., 2006, *ApJ*, 645, 1464
- Reed M. D., Armbrrecht E. L., Telting J. H., Baran A. S., Østensen R. H., Blay P., Kvammen A., Kuutma T., Pursimo T., Ketzer L., Jeffery C. S., 2018, *MNRAS*, 474, 5186
- Reed M. D., Baran A. S., Østensen R. H., Telting J. H., Kern J. W., Bloemen S., Blay P., Pursimo T., Kuutma T., Slumstrup D., Saajasto M., Nielsen L. D., Harmanen J., Winans A. J., Foster H. M., Rowe L., 2016, *MNRAS*, 458, 1417
- Reed M. D., Baran A. S., Quint A. C., Kawaler S. D., O’Toole S. J., Telting J., et al. 2011, *MNRAS*, 414, 2885
- Reed M. D., Baran A. S., Telting J. H., Østensen R. H., Jeffery C. S., Kern J. W., Ketzer L., Croke J., Slayton A., 2018, *Open Astronomy*, 27, 157
- Reed M. D., Foster H., Telting J. H., Østensen R. H., Farris L. H., Oreiro R., Baran A. S., 2014, *MNRAS*, 440, 3809

- Reed M. D., Harms S. L., Poindexter S., Zhou A. Y., Eggen J. R., et al 2011, *MNRAS*, 412, 371
- Reed M. D., Kawaler S. D., Zola S., Jiang X. J., Dreizler S., et al. 2004, *MNRAS*, 348, 1164
- Reed M. D., O’Toole S. J., Telting J. H., Østensen R. H., Heber U., Barlow B. N., Reichart D. E., Nysewander M. C., LaCluyze A. P., Ivarsen K. M., 2012, in Kilkenny D., Jeffery C. S., Koehn C., eds, *Fifth Meeting on Hot Subdwarf Stars and Related Objects Vol. 452 of Astronomical Society of the Pacific Conference Series, Multicolor Photometry and Time-resolved Spectroscopy of Two sdBV Stars*. p. 193
- Reed M. D., O’Toole S. J., Terndrup D. M., Eggen J. R., Zhou A.-Y., An D., Chen C.-W., Chen W. P., Lin H.-C., Akan C., Cakirli O., Worters H., Kilkenny D., Siwak M., Zola S., Kim S.-L., Gelven G. A., Harms S. L., Wolf G. W., 2007, *ApJ*, 664, 518
- Reed M. D., Shoaf K. A., Németh P., Vos J., Uzundag M., Baran A. S., Sahoo S. K., Jeffery C. S., Telting J. H., Østensen R. H., 2020, *MNRAS*, 493, 5162
- Reed M. D., Stiening R., 2004, *PASP*, 116, 506
- Reed M. D., Telting J. H., Ketzler L., Crooke J. A., Baran A. S., Vos J., Németh P., Østensen R. H., Jeffery C. S., 2019, *MNRAS*, 483, 2282
- Reed M. D., Yeager M., Vos J., Telting J. H., Østensen R. H., Slayton A., Baran A. S., Jeffery C. S., 2020, *MNRAS*, 492, 5202
- Ricker G. R., Vanderspek R., Winn J., et al. 2016, in *Proc. SPIE Vol. 9904 of Society of Photo-Optical Instrumentation Engineers (SPIE) Conference Series, The Transiting Exoplanet Survey Satellite*. p. 99042B
- Sahoo S. K., Baran A. S., Heber U., Ostrowski J., Sanjayan S., Silvotti R., Irrgang A., Uzundag M., Reed M. D., Shoaf K. A., Raddi R., Vuckovic M., Ghasemi H., Zong W., Bell K. J., 2020, *MNRAS*, 495, 2844
- Schuh S., Huber J., Dreizler S., Heber U., O’Toole S. J., Green E. M., Fontaine G., 2006, *A&A*, 445, L31
- Silvotti R., Uzundag M., Baran A. S., Østensen R. H., Telting J. H., Heber U., Reed M. D., Vücković M., 2019, *MNRAS*, 489, 4791
- Telting J., Østensen R., Reed M., Kiærad F., Farris L., Baran A., Oreiro R., O’Toole S., 2014, in van Grootel V., Green E., Fontaine G., Charpinet S., eds, *6th Meeting on Hot Subdwarf Stars and Related Objects Vol. 481 of Astronomical Society of the Pacific Conference Series, Low-Resolution Radial-Velocity Monitoring of Pulsating sdBs in the Kepler Field*. p. 287
- Telting J. H., Baran A. S., Németh P., Østensen R. H., Kupfer T., Macfarlane S., Heber U., Aerts C., Geier S., 2014, *A&A*, 570, A129
- Telting J. H., Østensen R. H., Baran A. S., Bloemen S., Reed M. D., Oreiro R., Farris L., Ottosen T. A., Aerts C., Kawaler S. D., Heber U., Prins S., Green E. M., Kalomeni B., O’Toole S. J., Mullally F., Sanderfer D. T., Smith J. C., Kjeldsen H., 2012, *A&A*, 544, A1
- Uzundag M., Baran A. S., Østensen R. H., Reed M. D., Telting J. H., Quick B. K., 2017, *MNRAS*, 472, 700
- Uzundag M., Vuckovic M., Németh P., Miller Bertolami M., Silvotti R., Baran A. S., Telting J. H., Reed M., Shoaf K. A., Østensen R. H., Sahoo S. K., 2021, *arXiv e-prints*, p. arXiv:2105.15137
- Van Grootel V., Charpinet S., Fontaine G., Brassard P., Green E., 2014, in van Grootel V., Green E., Fontaine G., Charpinet S., eds, *6th Meeting on Hot Subdwarf Stars and Related Objects Vol. 481 of Astronomical Society of the Pacific Conference Series, The Mass Distribution of sdB Stars Derived by Asteroseismology and Other Means: Implications for Stellar Evolution Theory*. p. 229
- Vos J., Østensen R. H., Vuckovic M., Van Winckel H., 2017, *A&A*, 605, A109
- Vuckovic M., Østensen R. H., Németh P., Bloemen S., Pápics P. I., 2016, *A&A*, 586, A146

Table 7. Spectroscopic and pulsation properties of published Kepler and TESS-observed sdBV stars organized by binary type, pulsation type, and then decreasing effective temperature. Column 1 provides the KIC, EPIC identifications, column 2 other identifications, column 3 provides the binary status where sdB is listed for single stars, sdB+WD for those with white dwarf companions, sdB+dM for those with M-dwarf main sequence companions and sdB+F or sdB+G for those with main sequence F or G companions. Column 4 provides the pulsation type where p are p-mode only pulsators, p+g are predominantly p mode hybrid pulsators, g are g-mode only pulsators, and g+p are predominantly g mode hybrid pulsators. Column 5 lists the g-mode $\ell = 1$ asymptotic period spacing, Column 6 the maximum amplitude and Column 7 the pulsation period of maximum amplitude. Columns 8 and 9 provide spectroscopic properties. Column 10 provides the binary period, column 11 provides the rotation rate and if two values are given, the first is derived from p-mode multiplets (for the envelope) and the second from g-mode multiplets (for deeper interior), and column 12 has references. The references are 1: Østensen et al. (2014), 2: Reed et al. (2020) 3: Baran et al. (2012), 4: Baran et al. (2017), 5: Foster et al. (2015), 6: Sahoo et al. (2020), 7: Charpinet et al. (2011), 8: Reed et al. (2011), 9: Uzundag et al. (2017), 10: Kern thesis 11: Kern et al. (2017), 12: Silvotti et al. (2019), 13: Bachulski et al. (2016), 14: this work, 15: Baran et al. (2015), 16: Ketzer et al. (2017), 17: Charpinet et al. (2019), 18: Reed et al. (2014), 19: Reed et al. (2018), 20: Reed et al. (2019), 21: Reed et al. (2020), 22: Telting et al. (2012); Kern et al. (2018), 23: Telting et al. (2014), 24: Østensen et al. (2014), 25: Reed et al. (2016), 26: Baran et al. (2016), 27: Østensen et al. (2010), 28: Baran et al. (2019), 29: Baran et al. (2018), 30: Pablo et al. (2012), 31: Baran & Winans (2012), 32: Østensen et al. (2012), 33: Jeffery et al. (2017) Notes: \diamond indicates stars with pulsation results only from the one month survey data. * No multiplets were detected for these stars which means spin periods longer than the observations, or that the pulsation axis is very nearly pole-on. In these cases, a lower limit of the spin period is provided. \dagger RV excesses have been measured for these stars (Sanjayan, S. et al. *in press*). K1718290 is listed as a blue horizontal branch (BHB) star.

Kepler ID	Other	Binary Status	Type	$\Pi_{\ell=1}$ (s)	A_{\max} (ppt)	$P_{A_{\max}}$ (μ Hz)	T_{eff} (K/1000)	$\log g$ (dex, cgs)	P_{orbit} (d)	P_{spin} (d)	Ref.
K2991276		sdB	p	–	2.25	8201.2	33.9 (2)	5.82 (4)	–	6.3	1
E248411044	UY Sex	sdB	p	–	4.89	7038.163	33.03 (20)	5.88 (1)	–	24.6 (3.5)	2
K10139564		sdB	p+g	207/310	7.95	5760.2	31.86 (0.13)	5.67 (3)	–	25.6 (1.8)/23.12 (62)	3
E211779126	2M 0856+1701	sdB	g+p	256	0.795	266.5	28.54 (8)	5.39 (1)	–	16/ > 45*	4
K3527751		sdB	g+p	266.4 (2)	7.11	255.7	27.82 (16)	5.35 (3)	–	15.3 (7)/42.6 (3.4)	5
T169285097	SB 815	sdB	g+p	265.09 (6)	1.642 (21)	258.1879 (29)	27.20 (55)	5.39 (10)	–	> 12*	6
K5807616 \diamond	KPD1943+4058	sdB	g+p	242.12 (62)	0.142	167.8	27.1	5.51	–	–	7,8
K10001893		sdB	g+p	268.0(5)	1.162	274.3	26.7	5.3	–	> 715*	9
K2569576	NGC 6791 B3	\dagger sdB	g+p	252.27 (66)	3.601	198.4	24.25 (46)	5.17 (5)	–	64.5 (8.2)	10
K2697388		sdB	g+p	240.06 (19)	33.29	156.4	23.39 (12)	5.29 (2)	–	41.9 (3.6)/52.8 (9.3)	11
E220641886	HD 4539	sdB	g+p	256.5	0.80	83.4	22.80 (16)	5.20 (2)	–	> 45*	12
E212707862		sdB	g	252.6 (1.1)	0.434	296.9	28.30 (16)	5.48 (3)	–	80	13
E215776487		sdB	g	247.8 (1.5)	0.489	197.0	27.86 (16)	5.45 (2)	–	–	14
K8302197		sdB	g	258.61 (62)	0.87	187.0	27.45 (20)	5.44 (3)	–	> 715*	15
E203948264		sdB	g	261.3 (1.1)	0.722	203.5	26.76 (61)	5.26 (9)	–	45.9 (8)	16
T457168745	PG0342+026	sdB	g	232.25 (30)	0.819 (21)	219.274 (6)	26.0 (1.1)	5.59 (12)	–	> 12*	17
T67584818	SB 459	sdB	g	259.16 (56)	1.72 (5)	207.314 (9)	24.9 (5)	5.35 (10)	–	> 12*	18
E218717602		sdB	g	263.55 (61)	3.71	168.1	24.47 (16)	5.17 (2)	–	–	19
K2437937	NGC 6791 B5	\dagger sdB	g	248.9 (1.3)	1.03	240.5	23.84 (68)	5.31 (9)	–	91.3 (14.1)	20
T278659026	EC 21494-7018	sdB	g	196.8	0.3184 (43)	249.269 (3)	23.72 (23)	5.65 (3)	–	> 12*	21
E217280630		sdB	g	207.35 (21)/195.28 (39)	0.39	75.5	22.77 (15)	5.01 (2)	–	7	22
K10670103		sdB	g	251.6 (2)	13.99	138.1	21.49 (54)	5.14 (5)	–	88 (8)	23
K1718290		BHB	g	276.3 (1)	.268	91.9	21.80 (14)	4.67 (3)	–	96.5	24
E211823779		sdB+F1V	p	–	2.052	7131.9538 (5)	36	6	–	11.5 (8)	25
E211938328	LB 378, EGGR 266	sdB+F6V	p	–	2.00	9648.77	32	5.8	635 (146)	21.5 (6)	26
E212508753	PG 1315-123	sdB+G	p+g	236.5 (1.3)	1.79	8116.1/497.62	36.23 (71)	5.61 (9)	> 100	15.83 (19)/16.18(57)	27
E220614972	PG 0048+091	sdB+G	p+g	207.45 (40)	1.792	5339.2/443.7	32.46 (27)	5.77 (6)	> 100	4.39 (48)/> 45*	28
T13145616	CD-28 $^{\circ}$ 1974	sdB+F/G	g+p	268.85 (32)	1.894 (91)	469.215 (12)	29.60 (38)	5.55 (9)	> 1000	> 12*	29
K11558725		sdB+WD	g+p	244.45 (32)	0.95	274.64187 (2)	27.91 (32)	5.41 (1)	10.055 (5)	44	30
K7668647	FBS1903+432	sdB+WD	g+p	248	0.42	194.5	27.7 (3)	5.50 (3)	14.174 (4)	50.5 (5)	31
K10553698		sdB+WD	g+p	263.15	1.367	202.0	27.42 (0.29)	5.44 (24)	3.387 (14)	42.9	32
E218366972		sdB+WD	g	254.95 (50)	2.742	249.8	28.16 (11)	5.44 (2)	5.92 (1)	> 45*	33
E201206621	PG 1142-037	sdB+WD	g	267.9 (10)	0.34	137.38	27.954 (54)	5.32 (1)	0.54109 (2)	> 45*	34
E211696659		sdB+WD	g	227.05 (56)	0.188	233.41	27.57 (30)	5.70 (3)	3.1604 (15)	28.4 (1.4)	35
K7664467		sdB+WD	g	263	0.495	247.0	27.44 (12)	5.38 (2)	1.5591 (6)	35.1 (6)	36

Table 7 – *continued*

Kepler ID	Other	Binary	Type	$\Pi_{\ell=1}$	A_{\max}	$P_{A_{\max}}$	T_{eff}	$\log g$	P_{orbit}	P_{spin}	Ref.
E246683636	V1405 Ori	sdB+dM	p+g	225	4.534	4703.538	31.4 (2)	5.47 (4)	0.398023 (0.3)	0.555 (29)/4.3	2
K9472174 [◇]	2M1938+4603	sdB+dM	p+g	255.63 (30)	3.01	3712.369	29.6	5.42	0.1258	0.1258	8,27
E246387816	EQ Psc	sdB+dM	g+p	233	2.21	495.8	28.69 (5)	5.64 (1)	0.80083 (1)	9.4	28
E228755638	HW Vir	sdB+dM	g+p	–	0.100	309.2	28.07 (5)	5.51 (1)	0.117	0.117	29
K11179657		sdB+dM	g+p	259.6 (14)	1.66	186.5	26	5.14	0.394	7.2	30,31
E246023959	PHL 457	sdB+dM	g+p	259 (2)	1.96	265.5	26.69 (6)	5.31 (1)	0.3128903 (4)	2.5/4.6	28
K2991403		sdB+dM	g	268.52 (74)	1.07	334.8	27.3	5.43	0.443	10.46	30,31
K2438324	NGC 6791 B4	sdB+dM	g	236.2 (2.1)	1.40	216.3	27.10 (82)	5.69 (10)	0.398	9.21 (18)	10,31